Fluorescence, Polarized Fluorescence, and Brewster Angle Microscopy of Palmitic Acid and Lung Surfactant Protein B Monolayers

Michael M. Lipp, Ka Yee C. Lee, Alan Waring,* and Joseph A. Zasadzinski
Department of Chemical Engineering, University of California at Santa Barbara, California 93106; and *Department of Pediatrics, King/Drew University Medical Center and Perinatal Laboratories, Harbor-UCLA School of Medicine, Los Angeles, California 90059 USA

ABSTRACT Fluorescence, polarized fluorescence, and Brewster angle microscopy reveal that human lung surfactant protein SP-B and its amino terminus (SP-B_{1-25}) alter the phase behavior of palmitic acid monolayers by inhibiting the formation of condensed phases and creating a new fluid protein-rich phase. This fluid phase forms a network that separates condensed phase domains at coexistence and persists to high surface pressures. The network changes the monolayer collapse mechanism from heterogeneous nucleation/growth and fracturing processes to a more homogeneous process through isolating individual condensed phase domains. This results in higher surface pressures at collapse, and monolayers easier to respread on expansion, factors essential to the in vivo function of lung surfactant. The network is stabilized by a low-line tension between the coexisting phases, as confirmed by the observation of extended linear domains, or "stripe" phases, and a Gouy-Chapman analysis of protein-containing monolayers. Comparison of isotherm data and observed morphologies of monolayers containing SP-B_{1-25} with those containing the full SP-B sequence show that the shortened peptide retains most of the native activity of the full-length protein, which may lead to cheaper and more effective synthetic replacement formulations.

INTRODUCTION

The primary function of lung surfactant (LS) is to form a monolayer at the alveolar air/water interface capable of lowering the surface tension to near zero values. An important corollary to this is that the monolayer must also be able to resist collapse upon the compression that accompanies expiration. This is achieved through the adsorption of a complex mixture of lipids and proteins to the interface, including dipalmitoylphosphatidylcholine (DPPC), unsaturated phosphatidylglycerol (PG), palmitic acid (PA), and lung surfactant-specific proteins SP-B and SP-C (two larger lung surfactant-specific proteins, SP-A and SP-D, are also present in lung surfactant but may not contribute as directly to surface activity as the hydrophobic surfactant proteins SP-B and SP-C). The presence of these monolayers greatly reduces the work of breathing and facilitates proper lung functioning by mechanically stabilizing the lungs against collapse (Shapiro, 1989).

The critical nature of these functions is manifested in neonatal respiratory distress syndrome (NRDS), where insufficient development of the LS system in premature infants, resulting in a lack of viable surfactant, has drastic consequences (including extremely high mortality rates). Proposed treatment methods for this syndrome have centered on the administration of exogenous natural surfactant mixtures directly into the lungs of the infants (Schwartz et al., 1994). However, sources of human LS, such as amniotic fluid, are low in quantity, and animal sources involve associated immunological and purity concerns (McLean et al., 1992). Additionally, the cost and effort of purifying LS proteins such as SP-B is a major concern in developing replacement formulations. The ideal surfactant replacement formulation would therefore involve a combination of synthetic lipids and either synthetic, genetically engineered, or highly purified natural proteins with improved efficacy and minimized costs.

In a related disease in adults, inactivation of LS is likely to be involved in the development of adult respiratory distress syndrome (Shapiro, 1989). This inactivation may be due to the presence of blood serum proteins in the lungs. The serum proteins, most likely albumin or fibrinogen, may compete with LS proteins for the anionic lipids in the monolayer, complex with or otherwise inactivate the protein, or may even displace the surfactant monolayer from the interface entirely (Cockshutt et al., 1991). Inactivation by blood serum proteins can also occur in severe cases of NRDS where extensive ventilation therapy causes significant lung trauma (Possmayer, 1988; Shapiro, 1989). As a result, it will be advantageous to tailor replacement formulations for optimum efficacy for specific treatments. The design of more effective synthetic lung surfactants is currently limited by the lack of a fundamental understanding of LS transport and spreading as well as the molecular level forces and interactions that determine the surface properties of lipid/protein monolayers. A close examination of binary mixtures of important minor lipid species such as PA with surfactant protein SP-B can reveal synergistic effects that would be impossible to predict from the phase behavior of either pure component. The behavior of minor species is also difficult to extract unambiguously from examining whole natural surfactant mixtures. A detailed knowledge of

Received for publication 26 August 1996 and in final form 28 February 1997.

Address reprint requests to Dr. J. A. Zasadzinski, Dept. of Chemical & Nuclear Engineering, University of California, Santa Barbara, CA 93106. Tel.: 805-893-4769; Fax: 805-893-4731; E-mail: gorilla@squid.ucsb.edu.

0006-3495/97/06/2783/22 $2.00

the role of each component of LS and their mechanisms of interaction in monolayers can lead to the design of simpler peptides and improved and less expensive replacement formulations. This knowledge can also help isolate the biophysical role of each component and the importance of the individual molecular features of each component, such as protein charge, hydrophobicity, or secondary structure.

The critical properties of the components of LS in the monolayer are exhibited in the relationship between molecular area and surface pressure (surface pressure, labeled π, is the difference between the surface tension of bare water (72 mN/m at ambient conditions) and the measured surface tension in the presence of a monolayer; the collapse pressure of a monolayer is the highest π attainable before the film collapses, or ejects material into a bulk phase) on compression and expansion, as shown in an isotherm. An ideal lung surfactant monolayer is compressible (fluidlike) at high areas per molecule, can attain low surface tensions upon compression, maintains these low tensions past collapse of the monolayer, and is capable of respreading rapidly and reversibly upon reexpansion. These properties are believed to be key to reducing the work of breathing and mechanically stabilizing the lungs in vivo (Shapiro, 1989).

Pure DPPC forms monolayers that can attain near-zero surface tensions and resist monolayer collapse up to surface pressures in excess of 70 mN/m. However, DPPC is a poor LS by itself, as its rigidity at physiological conditions causes it to adsorb slowly from solution and to respread poorly from a collapsed phase (Fleming and Keough, 1988). The unsaturated and anionic lipids found in LS are thought to act as emulsifiers and fluidizers that help the LS mixture to adsorb and respread rapidly. One such lipid, PA, is present in natural LS in relatively low amounts, but has been demonstrated to be a very important additive for the proper functioning of both natural and synthetic LS replacement formulations. The addition of up to 10 wt % PA to natural LS extracts obtained from both human and animal sources has been shown to result in a significant improvement of their properties both in vitro and in vivo (Tanaka and Tsunetomo, 1983; Tanaka et al., 1983; Ikegami et al., 1987; Cockshutt et al., 1991; Gorree et al., 1991; Fujiwara, 1992). For the design of synthetic-based LS mixtures, the addition of PA and SP-B to mixtures of unsaturated PG and DPPC has been shown to be essential to recapturing the surface activity of natural lung surfactants (Tanaka et al., 1986; Fujiwara, 1992).

The unsaturated anionic lipids and fatty acids present in natural and many synthetic replacement surfactants have relatively low collapse pressures, which has led to the hypothesis that they are "squeezed-out" of LS monolayers through some process of surface refining on compression (Cockshutt et al., 1991; Pastrana-Rios et al., 1994). However, Longo et al. have shown that the addition of the positively charged amphipathic amino terminal peptide sequence SP-$B_{1\text{-}25}$ of the native SP-B protein increases the collapse pressure of PA monolayers to values approaching that of DPPC, and creates a highly compressible region at high molecular areas similar to monolayers of whole LS (Longo et al., 1993). This change in the normal PA phase behavior effectively removes the driving force for the squeeze-out of PA, and potentially of other anionic fluidizing components such as PG, from LS monolayers.

Direct evidence of the mechanism by which this alteration of the PA phase behavior by SP-B takes place can add to our understanding of how LS works; very little is known about the nature of interactions between LS proteins and lipids in general (Hawgood and Shiffer, 1991; Weaver and Whitsett, 1991). Direct monolayer imaging techniques such as fluorescence (FM), polarized fluorescence (PFM), and Brewster angle microscopy (BAM) can shed light on the mechanism of these interactions and lead to the development of a detailed structure-function relationship among all of the components of LS. FM, PFM, and BAM are relatively recent techniques for monolayer imaging, but have already resulted in a tremendous increase in our understanding of the phase behavior of lipid monolayers (Hénon and Meunier, 1991; Hönig and Möbius, 1991; McConnell, 1991; Knobler and Desai, 1992; Möhwald, 1993). However, little FM, PFM, or BAM work has been done on the lipids and proteins common to lung surfactants (Nag et al., 1991; Perez-Gil et al., 1992; Nag and Keough, 1993; Nag et al., 1994; Taneva and Keough, 1994; Lipp et al., 1996).

In an earlier paper, we demonstrated using FM that the addition of SP-B protein had a significant effect on the phase behavior of PA monolayers (Lipp et al., 1996). Upon addition to PA monolayers, both the full-length and amino-terminal proteins led to the formation of a new bright fluid phase, which shifted the condensed-type PA isotherm into a more fluidlike isotherm with an increase in the liftoff area and monolayer compressibility. Fluorescence images showed that the fluid phase formed a network that partitioned and segregated the condensed phase domains. The average condensed phase domain size was greatly reduced in the presence of protein at all conditions, and the domains remained isolated from each other right up to collapse of the monolayer. This resulted in a significant increase in the collapse pressure of these monolayers, inducing the formation of small, homogeneously distributed collapsed phase domains and increasing the reversibility of the collapse event. This was in contrast to the irreversible growth of large, dendritic collapsed phase domains at low pressures observed in pure PA monolayers on pure water subphases, and appeared to be a direct effect of the partitioning of the condensed domains by the bright phase network.

In this paper, we utilize several different experimental techniques in conjunction with FM to further probe the nature of the alteration of the phase behavior of PA by SP-B. We first use a combination of FM and PFM to examine the complete phase behavior of the PA/SP-B system as a function of temperature and subphase conditions. PFM can be used to identify regions of tilted liquid crystalline phases in lipid monolayers. By using PFM, we show that the presence of tilted phases in both the condensed and collapsed phases of pure PA monolayers on a pure water

subphase may help to explain the low surface pressure and irreversible nature of collapse; their absence upon addition of SP-B protein may explain the shift to a higher-pressure, more reversible collapse event. We also identify a second, bulk-fracturing collapse mechanism for pure PA monolayers on buffered saline subphases, and show that this collapse event is also shifted to a more homogeneous, higher-pressure nucleation and growth process in the presence of protein. We use fluorescently labeled SP-B_{1-25} protein to examine the partitioning characteristics of the protein with respect to the observed monolayer phases. Simultaneous observation of the fluorescence from both lipid and protein-labeled molecules (using fluorophores emitting at different wavelengths) reveals that the protein partitions preferentially into the fluid monolayer phases that form the network around the condensed phase PA-rich domains under all experimental conditions. We also use fluorescently labeled SP-B_{1-25} to identify other specific protein-induced effects, including the formation of linear stripelike phases consisting of elongated domains, which indicates a reduction in line tension between the coexisting phases (surface tension is the force per unit area exerted on the two-dimensional interface between two coexisting phases in three dimensions; similarly, line tension is the force per unit length exerted on the one-dimensional interface between two coexisting phases (here termed the interphase perimeter) in two dimensions). Additionally, a concern with the use of both FM and PFM is the effect of the presence of the fluorophore on the observed phase behavior of the monolayer. In this paper, we also use BAM (a technique for imaging Langmuir monolayers that does not require the presence of fluorescently labeled molecules) to confirm that the addition of foreign fluorescent probes to the system in small quantities does not influence the observed results.

Finally, we employ Gouy-Chapman theory to attempt to explain the effect of the electrostatic state of the monolayer on the observed phase behavior. We use the traditional Gouy-Chapman theory to show that the shift in the collapse mechanism of pure PA to a bulk fracturing process on buffered saline subphases is directly due to the ionization of the monolayer. Additionally, our earlier results indicated that the presence of protein in PA monolayers resulted in a low-line tension between the coexisting phases in the monolayer, allowing for the large amount of perimeter between the condensed phase and fluid phase network accompanying the increase in condensed phase domain density, and also leading to the formation of elongated stripe phases under certain experimental conditions (Lipp et al., 1996). Current theories predict that the equilibrium width of condensed domains depends on the ratio of the line tension of the domain versus the electrostatic dipole density within a single domain (with respect to the surrounding phase) and between the condensed phase domains themselves (McConnell, 1991; Möhwald et al., 1995; Riviere et al., 1995; Seul and Andelman, 1995; McConnell and De Koker, 1996). The nucleation density of condensed domains at the fluid to condensed phase transition will also likely depend on the ratio of the line tension to the electrostatic free energy of the critical nuclei. Higher domain densities and stripelike phases thus can occur as a result of either a lowered line tension or an increase in the dipole density difference within or between domains. However, the line tension between two-dimensional phases is a difficult parameter to predict theoretically or measure directly, in particular for systems containing condensed phases with a nonzero electrostatic dipole contribution perpendicular to the interface (Benvegnu and McConnell, 1992; Muller and Gallet, 1992). By performing a modified Gouy-Chapman analysis on the PA/SP-B monolayer system, we predict that the presence of up to 20 wt % SP-B protein has little effect on the electrostatic dipole density of the condensed phase nuclei or the equilibrium condensed phase domains themselves, which indicates that a lowering of the line tension is the driving force behind the increase in nucleation density of the condensed phase domains and the formation of stripe phases. The Gouy-Chapman analysis also allows us to predict the local pH in the vicinity of the surface as a function of molecular area and subphase conditions, which may have a significant effect on the protein conformation in the monolayer.

MATERIALS AND METHODS

Chemicals

Palmitic acid (Sigma Chemical Co., St. Louis, MO; >99% pure) was used without further purification. *N*-7-Nitrobenz-2-oxa-1,3-diazol-4-yl-hexadecylamine (NBD-HDA, Molecular Probes Inc., Eugene, OR) was also used as obtained. All subphases were prepared using purified water obtained from a Milli-Q system (Millipore Co., Bedford, MA). Physiological subphases were made containing 0.15 M NaCl and a 2 mM $NaHCO_3$ buffer (pH = 6.9).

Peptide synthesis

The native human 78-amino acid sequence of surfactant protein (SP-B_{1-78}) was synthesized on a 0.25 mmol scale with an ABI 431A peptide synthesizer (Applied Biosystems, Foster City, CA) using Fmoc chemistry (Lipp et al., 1996). In each sequence, the charged residues are indicated with a "+" or a "−" sign:

```
      1          +   ++       +25
NH2-FPIPLPYCWLCRALIKRIQAMIPKG
     +      +                50
   ALRVAVAQVCRVVPLVAGGICQCLA
    −+     −    +       +   + 78
   ERYSVILLDTLLGRMLPQLVCRLVLRCS-COOH
```

A Wang Fmoc-L-Serine (OtBu) resin (Applied Biosystems) was employed for the synthesis. Amino acid residues 26 to 59 were double coupled, while all other residues were single coupled. After cleavage from the resin, the peptide was purified by reverse phase HPLC with a C4 column (Vydac, Hesperia, CA) using a water-acetonitrile gradient containing 0.1 vol % trifluoroacetic acid (TFA). The composition of the purified material was verified by quantitative amino acid analysis (UCLA Protein Microsequencing Facility), and the expected molecular weight of the reduced monomer was confirmed by electrospray mass spectrometry (UCLA Center for Molecular and Medical Mass Spectrometry). The formation of disulfide bonds was facilitated using EKATHIOX resin (Ekagen Corp., Palo Alto, CA). Oxidation with EKATHIOX resin was carried out by the addition of

a 1 mM peptide solution of trifluoroethanol/water (8:2 v/v) to a 10-fold molar excess of the resin active group to peptide thiol. The reaction was allowed to proceed for 6 h before the peptide in solution was separated from the resin by centrifugation (1000 × *g*, 10 min). The mass of the oxidized monomer was confirmed by matrix-assisted laser-induced desorption and ionization time-of-flight (MALDI-TOF) mass spectrometry.

Synthetic peptide representing the NH_2-terminal amino acid sequence (residues 1–25)–OH was synthesized using Fmoc chemistry with HBtu activation for coupling (Fields et al., 1991). In this sequence, the charged residues are indicated with a "+" sign

```
          1          +   ++       +25
NH2-FPIPLPYCWLCRALIKRIQAMIPKG-COOH.
```

SP-$B_{1\text{-}25}$ was assembled stepwise on 0.25 mmol scale using a Fmoc-glycine Wang resin (Applied Biosystems) and cleaved as described previously (Gordon et al., 1996).

The crude peptides were purified by reverse phase HPLC using a water-acetonitrile gradient containing 0.1 vol % TFA. Peptides were chromatographed using a linear gradient with an initial mobile phase of 20:80 vol/vol acetonitrile/water containing 0.1 vol % TFA that was programmed to 100% acetonitrile with 0.1 vol % TFA after 1 h. The elusion of the material was monitored at 280 nm. HPLC solvents and ion pairing agents were removed from the purified peptides by vacuum centrifugation, followed by lyophilization from acetonitrile/10 mM HCl (1:1 vol/vol). The expected molecular mass for SP-$B_{1\text{-}25}$ was obtained by fast atom bombardment mass spectrometry (UCLA Center for Molecular and Medical Mass Spectrometry, Los Angeles, CA).

The fluorescein derivative of SP-$B_{1\text{-}25}$ (F-SP-$B_{1\text{-}25}$) with linkages at cysteine residues 8 and 11 was synthesized by slowly adding a fivefold excess of fluorescein-5-maleamide (Molecular Probes, Eugene, OR) in dimethylformamide to the peptide in 10 mM–100 mM phosphate buffer at pH 6.5. The mixture was bath sonicated for 5 min and vortexed for 1 h at 25°C. The reaction was then quenched with a twofold excess of cysteine and the reaction mixture was dialyzed against distilled water overnight. The resulting product was then freeze-dried and purified by reverse phase HPLC as described above.

METHODS

Stock spreading solutions were made with either pure chloroform (for PA) or 4:1 vol/vol chloroform-methanol (for protein). Actual spreading solutions were made by mixing aliquots of the stock solutions in the desired ratios. Solutions were spread dropwise on the surface using a microsyringe, and at least 20 min was given for complete solvent evaporation. Monolayers were compressed at rates in the range 0.02–0.10 $Å^2 \cdot molec^{-1} \cdot s^{-1}$; the speed was held constant during a particular series of runs. We did not detect any difference in the equilibrium features of the isotherms, such as the compressibility of phases and points of initiation and termination of phase transitions when experiments were conducted at different compression speeds in this range. For kinetically limited events such as nucleation of condensed domains at the onset of phase transitions, we observed dependence on the speed of compression as well as trough geometry. However, by holding these two variables constant during a given set of experiments, quantitative comparisons could be made between different monolayers. For the experiments discussed below, all monolayers were compressed at a speed of 0.02 $Å^2 \cdot molec^{-1} \cdot s^{-1}$, and lipids were spread at an initial area of ~62 $Å^2$/molec.

A schematic of the FM/PFM/BAM assembly is shown in Fig. 1. The experimental system consisted of a Langmuir trough milled from a solid piece of Teflon, with a working surface area of 112 cm^2 and a subphase volume of 150 ml. A Teflon barrier that ran linearly along the top edge of the trough well was driven by a DC motor with a resolution of 0.1 μm (which translates to a resolution of $\sim 10^{-3}$ $Å^2 \cdot$ mol). The surface pressure was measured via a Wilhelmy plate system (Riegler & Kirstein, Wiesbaden, Germany). Temperature control of the subphase was achieved through the use of thermoelectric heating elements, (Marrow Industries, Dallas, TX), located between a copper plate bonded to the bottom of the trough and a constant temperature reservoir; the temperature of the subphase could be maintained in the range of 10 to 50°C (±0.2°C).

For the fluorescence system, a Nikon fluorescence microscope (A. G. Heinz Co., Irvine, CA) utilizing a 40× power long working distance objective coupled to a silicon intensified target (SIT) camera (DAGE-MTI, Sunnyvale, CA) was used for imaging. The microscope allowed for the quick exchange of two fluorescence cube assemblies, making the simultaneous monitoring of different emission wavelengths possible. Conductive glass (Delta Technologies, Dallas, TX), that was resistively heated to eliminate condensation on the objective and to reduce convective air currents, was placed over the well during experiments. For the polarized fluorescence operation, a Coherent (Palo Alto, CA) argon ion laser provided *p*-polarized light incident on the monolayer at an oblique angle. With PFM, the fluorescence intensity of tilted phases depends on the relative orientation of the electric field vector of the incident beam with respect to the molecular tilt direction. The plane of incidence of the laser beam could be instantaneously rotated by 180° to detect regions of different tilt direc-

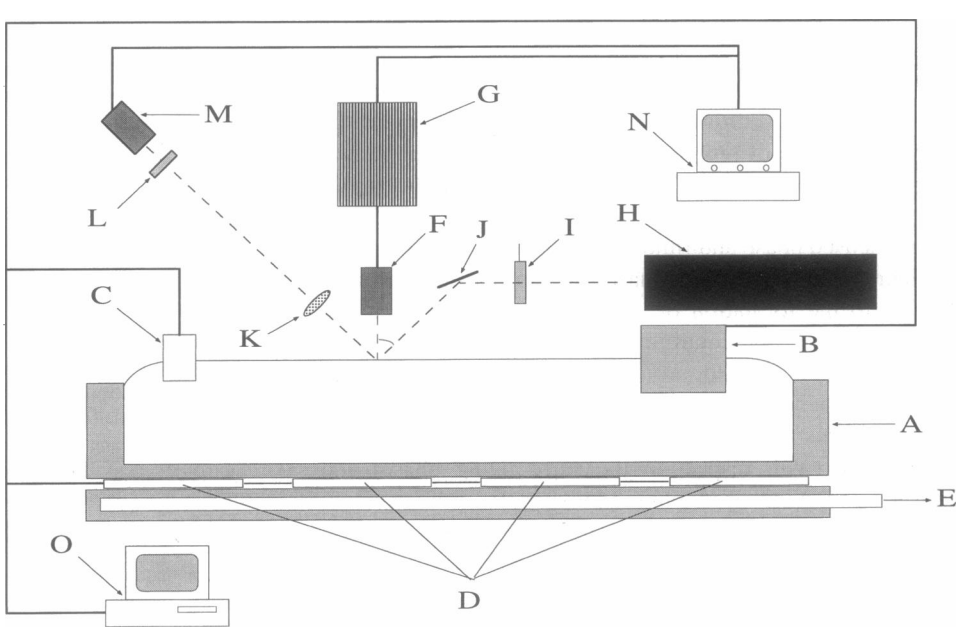

FIGURE 1 A diagram of the FM/PFM/BAM assembly. The labeled parts are: (*A*) Teflon trough; (*B*) Teflon barrier; (*C*) Wilhelmy plate system; (*D*) thermoelectric heating elements; (*E*) outlet to water bath; (*F*) fluorescence objective; (*G*) silicon intensified target (SIT) camera; (*H*) argon ion laser; (*I*) polarizer; (*J*) mirror; (*K*) lens; (*L*) analyzer (polarizer); (*M*) CCD camera; (*N*) VCR/monitor system; (*O*) computer (plus interfacing hardware, power supplies, etc.).

tion. For operation in Brewster angle mode, the argon ion laser provided *p*-polarized light incident on the monolayer at the Brewster angle. A long focal length lens system was used to collect the weakly reflected light, and a rotatable polarizer positioned posterior to the objective was used as an analyzer to improve contrast in the image. A CCD camera (DAGE-MTI) was used for imaging; it was mounted on a rotary stage to allow the CCD chip to be positioned to compensate for longitudinal distortion effects produced by imaging at the Brewster angle. For all three systems, images were recorded via a JVC S-VHS VCR (Elmwood Park, NJ) and digitized for analysis. The details of this setup are presented elsewhere (Lipp et al., 1997).

Image analysis was performed utilizing a combination of NIH Image and Adobe Photoshop software. For the calculation of nucleation densities of condensed domains at the beginning of expanded-to-condensed phase transitions, at least three separate experimental runs were sampled for each particular set of experimental conditions. Ten frames were chosen randomly for each run, and an average nucleation density was calculated. For the calculation of average domain radii and interphase perimeter at a particular point in an isotherm, images from three separate experimental runs were obtained. The raw images were first filtered and then thresholded, and the NIH image was used to calculate the average domain radius. An average perimeter per domain was then calculated, and multiplied by the domain density to give an average value of the interphase perimeter per monolayer area.

RESULTS

PA/SP-B_{1-25} monolayers on a pure water subphase at 16°C

The addition of SP-B_{1-25} protein to PA monolayers at all experimental conditions resulted in dramatic alterations in phase behavior. The first set of monolayers were deposited on a pure water subphase at a temperature of 16°C, which is well below the triple point of PA (~25°C) on a pure water subphase (in the case of monolayers, the triple point denotes the location in the phase diagram where the two-dimensional equivalents of the solid (liquid-condensed), liquid (liquid-expanded), and gaseous phases all coexist in equilibrium). As only the gaseous and liquid condensed (lc) phases existed prior to the solid phase at this temperature, these conditions allowed for an unambiguous determination of the new phases seen and made it possible to probe the fluidizing effects of the peptide on PA monolayers. Surfactant monolayers at the air-water interface typically progress through several phases upon compression, depending on the nature of the amphiphile, subphase conditions, and temperature. At sufficiently large areas per molecule, all monolayers exist in a gaseous state, in which the individual molecules are isolated on the surface with their hydrophobic tails in contact with the subphase. Below the triple point, PA monolayers underwent a transition from a coexistence between gaseous and lc phases at large surface area per molecule to a uniform lc phase at the lift-off point (designated by *a* in Fig. 2 *A*). Upon further compression, this lc phase transformed into a solid-condensed phase at a pressure ~21 mN/m and an area of ~19 Å^2/mol (Fig. 2 *A*, point *b*), and eventually collapsed by forming a three-dimensional phase above the monolayer as the area was decreased further (Fig. 2 *A*, point *c*).

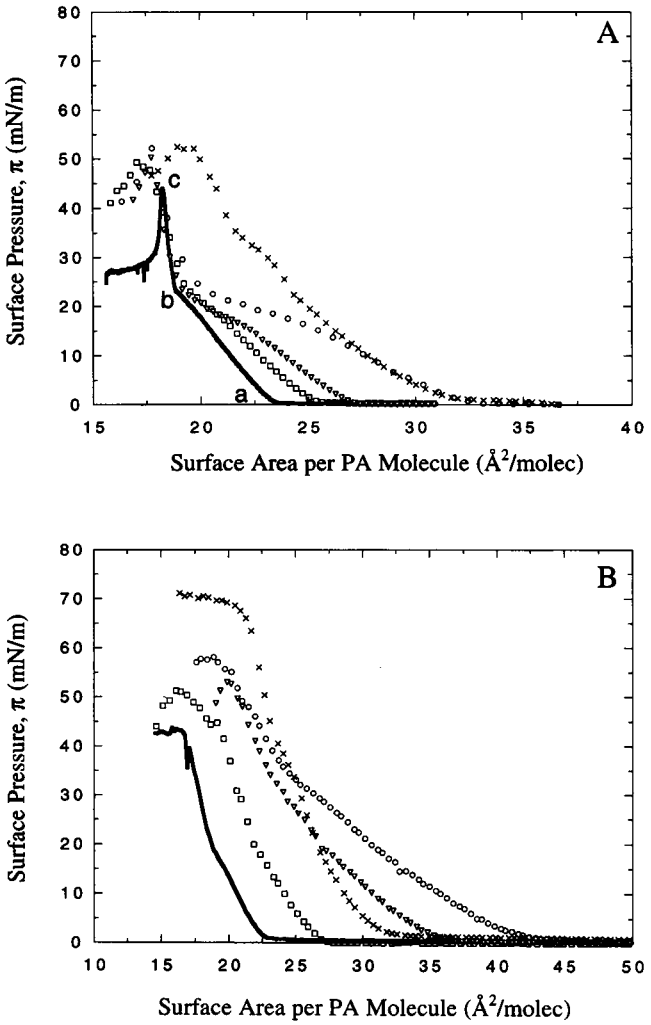

FIGURE 2 Surface pressure versus area per PA molecule isotherms as a function of peptide weight fraction. Isotherms of PA at 16°C on (*A*) pure water (pH = 5.5) and (*B*) buffered saline (0.15 M NaCl, pH = 6.9) containing: 0 (—), 5 (□), 10 (▽), and 20 (○) wt % SP-B_{1-25}, and 20 (×) wt % SP-B_{1-78}. The isotherm of PA alone shows two distinct nongaseous phases: a compressible liquid condensed (lc) phase (segment *a* to *b*) and an incompressible solidlike phase (segment *b* to *c*). In addition to these phases, addition of up to 20 wt % SP-B_{1-25} leads to the appearance of a flattened, highly compressible region at elevated pressures.

With the addition of the fluorescent probe NBD-HDA, this sequence of phases was visualized as a progression from a coexistence of dark gas phase and gray lc phase at a high area per molecule, with the dark phase disappearing at the lift-off point and the film becoming a homogeneous sheet of gray lc phase (Fig. 3 *A*). The homogeneity persisted through the second order lc-solid transition up to collapse of the monolayer, which occurred at a pressure and area of 40 mN/m and 17.8 Å^2/mol, respectively. Collapse of the monolayer followed a nucleation and growth mechanism; individual isolated nuclei appeared heterogeneously across the film and grew into large crystallinelike structures upon compression past the collapse point (Fig. 3 *B*). These collapsed phase domains consisted of regions of different tilt

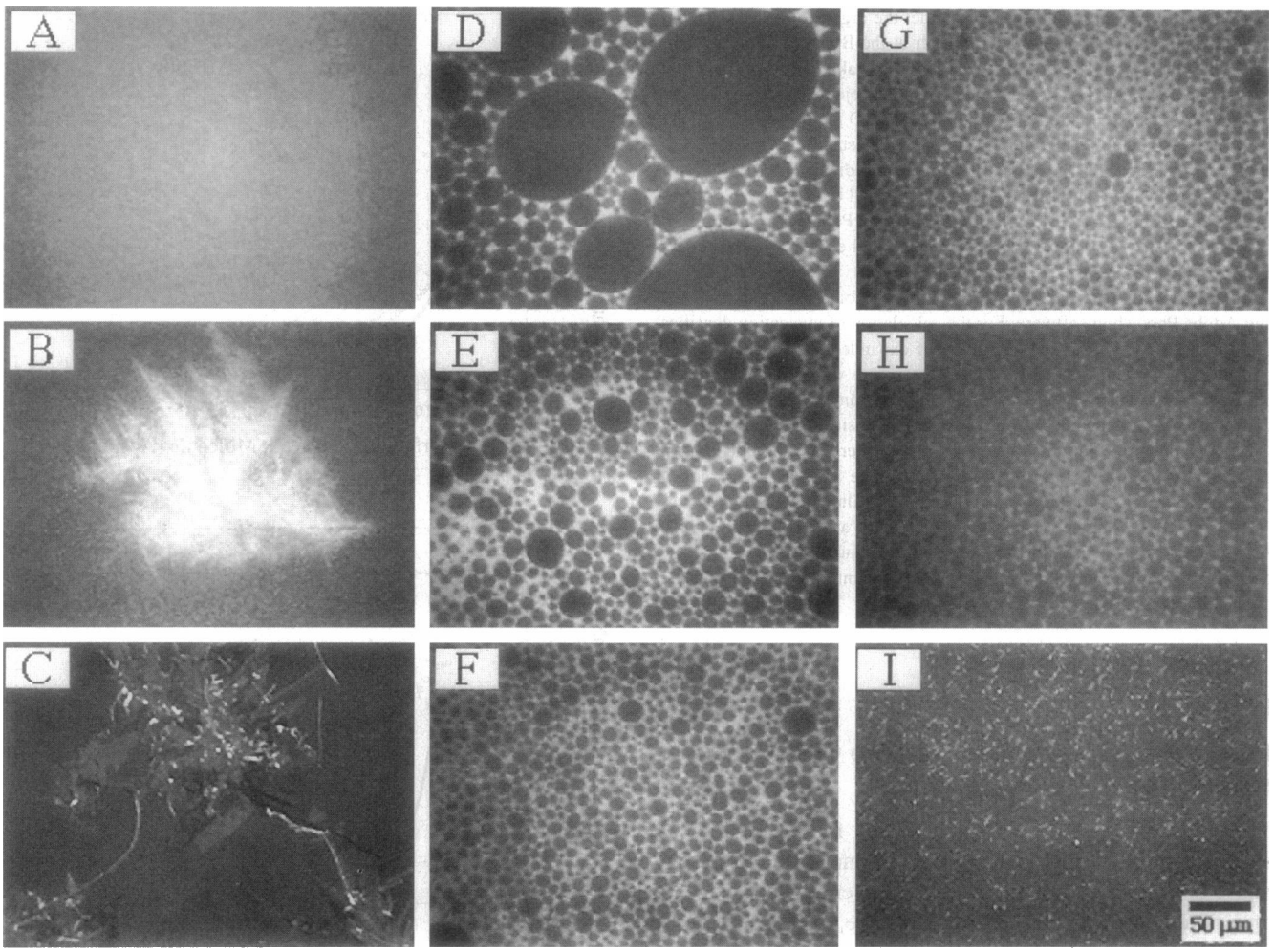

FIGURE 3 Images of PA and PA/SP-$B_{1\text{-}25}$ films containing 0.5 mol % NBD-HDA on a pure water subphase at 16°C. (*A*, *B*) Fluorescence images of a pure PA film (*A*) at the lift-off point (designated by *a* in Fig. 2 *A*), consisting entirely of lc phase, and (*B*) the film post-collapse, showing dendritic growth of a crystalline phase above the monolayer. (*C*) Polarized fluorescence image of a collapsed phase domain, showing the existence of tilt contrast within the collapsed phase. (*D–F*) Fluorescence images taken at the lift-off point of PA films containing (*D*) 5, (*E*) 10, and (*F*) 20 wt % SP-$B_{1\text{-}25}$, showing the reduction in the average condensed domain size with increasing amounts of protein. (*G–I*) Images from a progression of a 20 wt % SP-$B_{1\text{-}25}$ film. (*G*, *H*) Fluorescence images showing (*G*) the coexistence of lc and fluid phases at an area per molecule of 25 $Å^2$, and (*H*) the persistence of the bright phase network up to monolayer collapse. (*I*) A polarized fluorescence image of the film post-collapse, showing nucleation and growth of small collapse structures above the film [in contrast to the collapsed phase morphology shown in (*C*)] and a lack of tilt contrast within the collapsed phase domains.

direction, as evidenced by the presence of tilt contrast upon viewing with PFM (Fig. 3 *C*), although the underlying monolayer was still in the untilled solid phase. Upon expansion of the collapsed film, the monolayer did not follow the same progression as during compression. The film was very rigid and the collapsed domains did not break up upon re-expansion. The underlying solid phase did not readily expand either, instead it fractured at several locations. After the film fractured, the surface pressure immediately dropped to near zero, exhibiting a large hysteresis from the compression isotherm.

The addition of protein in amounts ranging from 5 to 20 wt % resulted in a shift in the liftoff points of the isotherms to substantially higher areas per PA molecule (see Fig. 2 *A*), indicating that the protein was retained in the monolayer. The protein induced the formation of a new bright fluid phase at high surface areas, resulting in a three-phase coexistence with gas and lc phase. Upon compression, the gas phase disappeared at the liftoff point, while the lc and bright phases persisted; a lattice of gray lc domains in a bright fluid background was visible throughout the previously one-phase lc region (see Fig. 3 *D–F*). The bright phase inhibited the formation of the lc phase and broke it up into small domains. As the concentration of protein was increased, the size of the lc domains progressively decreased (Fig. 3 *D–F*). The magnitude of the slope of the isotherm gradually decreased as the protein concentration was increased, indicating that the compressibility of the films increased (Fig. 2 *A*). The formation of the plateau region in Fig. 2 *A* as the protein concentration reached 20 wt % corresponded to the reduction of bright fluid phase from the interstitial regions (Fig. 3, *G* and *H*). For all concentrations,

the "bulk" regions of bright phase completely disappeared once the isotherm reached a kink point at a location similar to the lc-solid transition point in the pure film (see point *b* in Fig. 2 *A*). However, the network of bright phase that originally surrounded the original lc domains persisted throughout the solid phase of the monolayer right up to collapse.

The presence of the protein had a dramatic effect on the collapse behavior of these monolayers. The collapse pressures were raised significantly upon the addition of protein, reaching a value of 55 mN/m for the 20 wt % SP-B_{1-25} film (Fig. 2 *A*). Collapse followed a more homogeneous pathway as well: small collapse structures appeared across the monolayer with a high nucleation density and without evidence of tilt contrast (Fig. 3 *I*), as opposed to the large, tilted structures observed for the pure PA film (see Fig. 3 *C*). Upon expansion the monolayer morphology was more reversible, with the bright phase reappearing in a similar fashion as before collapse. The hysteresis between compression-expansion cycles was greatly reduced as well, the isotherm was retraced with the same features with only a small area offset (data not shown).

PA/SP-B_{1-25} monolayers on a buffered saline subphase at 16°C

For the next set of experiments, a subphase more representative of physiological conditions consisting of buffered saline (0.15 M NaCl, pH = 6.9) was employed; the temperature was kept at 16°C to allow for a direct comparison with the first set of experiments. Isotherms corresponding to the same protein concentrations employed in the first set of experiments are shown in Fig. 2 *B*. Under these conditions, PA monolayers containing 0.5 mol % NBD-HDA showed similar behavior to the pure water case (i.e., a gas → lc → solid phase progression), and the presence of protein had a similar effect on the fluidity of these films. However, a new morphological feature was observed for the 20 wt % SP-B_{1-25} film. Immediately after spreading (at an area of ~62 $Å^2$/mol), a gas-fluid-lc coexistence appeared as before, with the gas/fluid phase appearing as circular domains of gas phase in a bright fluid matrix. However, after a few minutes, regions of bright stripes were formed throughout this phase (Fig. 4 *A*). These stripes were of a constant width (on the order of microns), and formed labyrinthine patterns over large areas of the surface. The stripe regions coexisted with areas of lc phase in a bright fluid matrix. Upon compression, these stripes transformed back into circular domains (Fig. 4 *B*). At elevated pressures, the extent of perimeter between the fluid and condensed phases increased, resulting in a formation of a meshlike network that persisted until monolayer collapse (Fig. 4 *C*).

The amount of stripe phase present was correlated with the amount of protein added; only a few isolated stripe phase domains were seen in the 10 wt % SP-B_{1-25} film (data not shown) while large regions of stripe phase were observed in the 20 wt % SP-B_{1-25} film. To further confirm this correlation, a film of 30 wt % SP-B_{1-25} in PA was prepared; stripe phases of similar dimensions appeared at the same conditions, but the percentage of stripe phases at high surface areas was increased substantially with regions of very dense stripes coexisting with foamlike regions that contained isolated stripes connected to each other at vertices in a gas matrix (Fig. 4 *D*). Observation of a pure monolayer of fluorescein-labeled SP-B_{1-25} (F-SP-B_{1-25}) revealed that the formation of the stripe phase was due to the protein. At low pressures, the F-SP-B_{1-25} monolayer consisted entirely of striped domains of similar dimensions as those seen in the 20 and 30 wt % PA/SP-B_{1-25} films (Fig. 4, *E*, *F*).

Changing the subphase to buffered saline had a significant effect on the collapse behavior of the pure PA films. Collapse occurred at a higher pressure than on the pure water subphase. Instead of following a nucleation and growth mechanism, the film fractured in several locations leading to the appearance of elongated bright cracks, which in some cases were millimeters in length (Fig. 4 *G*). This fracturing process was irreversible, with the cracks persisting upon re-expansion of the film to low pressures. The addition of SP-B_{1-25} drastically altered both the collapse pressure and the collapse mechanism of PA monolayers. The collapse pressure was significantly higher than that of a protein-free PA monolayer under the same conditions, reaching values of ~70 mN/m for the 20 wt % SP-B_{1-25} film. The bright phase network persisted to high pressures (Fig. 4 *H*), and the collapse mechanism shifted to a more homogeneous, nucleation-type event; individual small nuclei appeared homogeneously across the film and grew to a finite size upon further compression (Fig. 4 *I*).

PA/SP-B_{1-25} monolayers on a pure water subphase at 28°C

Isotherms (Fig. 5 *A*) and FM images (Fig. 6) were obtained for PA/SP-B_{1-25} mixed monolayers at 28°C (which is a few degrees above the triple point of PA on a pure water subphase). The phase behavior at this temperature was similar to that at 37°C. For pure PA monolayers above the triple point temperature at these conditions, the progression of phases on both pure water and buffered saline subphases was gas → liquid-expanded (le) → lc → solid. Above the triple point, monolayers of pure PA exhibited a gas-le phase coexistence at large areas per molecule, with dark, circular domains of gas phase distributed in a bright background of le phase (in the gas phase the hydrocarbon chains of the amphiphiles are in contact with the subphase; since NBD-HDA quenches in an aqueous environment the gas phase appear dark). On compression, the gas phase disappeared and a uniform, bright le phase remained at the liftoff point. Further compression resulted in an increase in the surface pressure until lc domains nucleated from the le phase and the corresponding le-lc coexistence plateau was reached (Fig. 6 *A*). The lc domains grew in size on continued

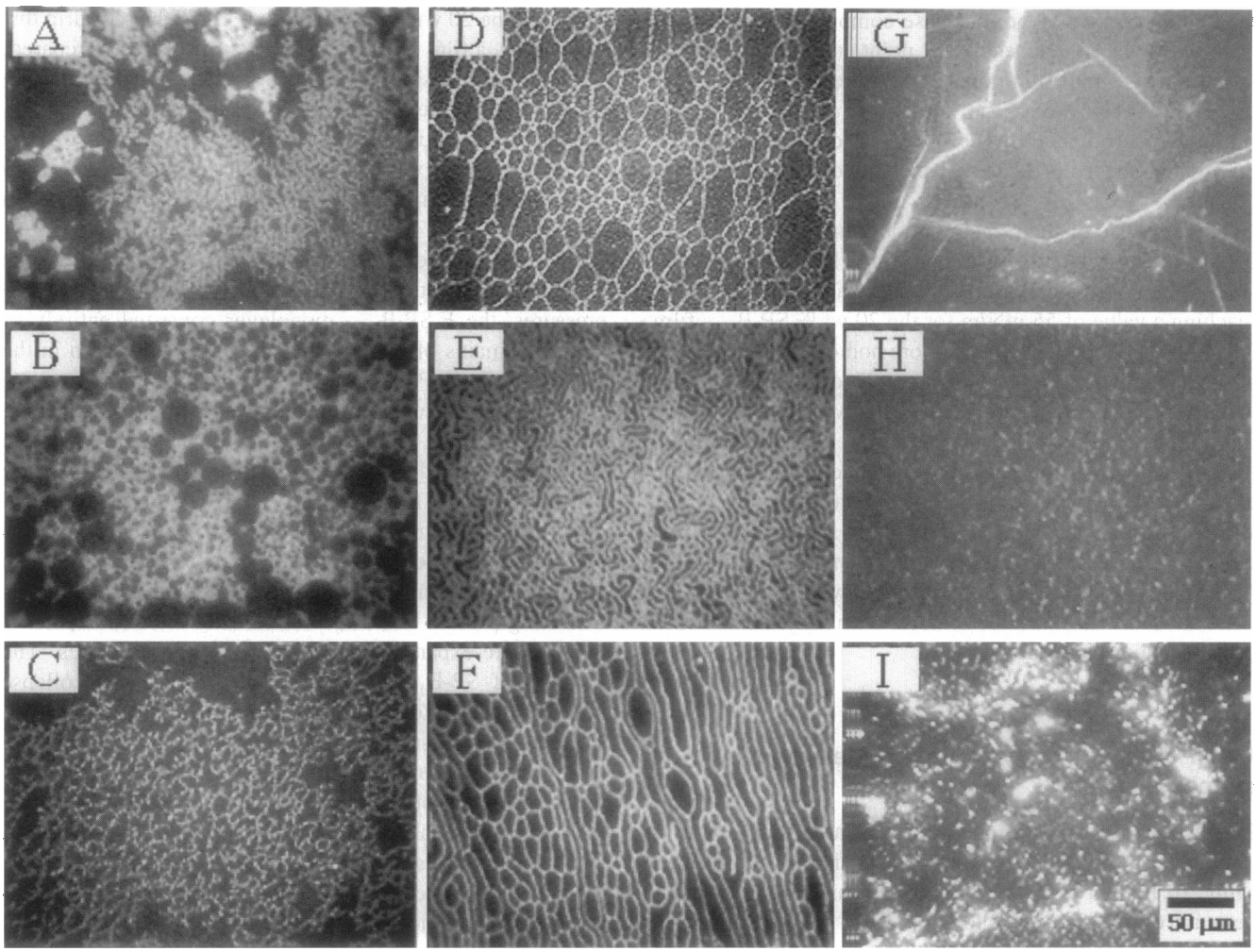

FIGURE 4 Fluorescence images of PA and PA/SP-B_{1-25} films containing 0.5 mol % NBD-HDA on a buffered saline (0.15 M NaCl, pH = 6.9) subphase at 16°C. (*A–C*) Images of a PA/20 wt % SP-B_{1-25} film showing (*A*) the formation of an extended stripe phase at high areas per molecule, (*B*) the conversion of the extended domains into circular domains upon compression, and (*C*) the eventual formation of an elongated mesh of bright phase surrounding the condensed phase domains prior to collapse of the monolayer. (*D–F*) Additional images of stripe phases occurring in various films, including (*D*) the formation of a foamlike region of stripe phase in a 30 wt % SP-B_{1-25} film at high areas, (*E*) the formation of a stripe phase in a pure fluorescein-SP-B_{1-25} film at high areas on a pure water subphase, and (*F*) the formation of a foam-like network in the same film upon expansion. (*G–I*) Images of collapse behavior of PA and PA/SP-B_{1-25} films, showing (*G*) the bulk fracture of a pure PA film upon collapse, (*H*) the existence of a bright phase mesh immediately prior to collapse of a PA/20 wt % SP-B_{1-25} film, and (*I*) the formation of the collapsed phase domains in the same film.

compression, but stayed separated from each other until the remaining le phase disappeared. The lc domains then merged into a continuous sheet (Fig. 6 *B*), transforming into a solid-condensed phase that eventually collapsed. Similar to the films imaged at 16°C on a pure water subphase, collapse occurred by a nucleation and growth mechanism; scattered nuclei appeared at low density across the film at the collapse point. Tilted, crystalline collapsed phase domains grew from these nuclei upon compression past the collapse point (Fig. 6 *C*). These collapsed structures eventually reached very large sizes, covering the whole field of view (200 × 350 μm) in some cases.

The addition of protein in amounts ranging from 5 to 20 wt % again acted to fluidize these monolayers. The films exhibited a gas-fluid phase coexistence on initial spreading at large areas per molecule, with a uniform, bright fluid phase remaining at the lift-off point (For pure lipid monolayers, an le phase refers to a fluid state of a lipid monolayer for which the molecules are in contact with each other and the hydrocarbon chains are liquidlike. These conditions do not seem to change when protein is added. However, since this phase is seen to contain significant amounts of protein and the term le strictly refers to a lipid phase, the term fluid phase will be used instead.). Since the lc domains now nucleated from a uniform phase on compression, the effect of the protein on the nucleation and condensation process was more readily observed. The addition of increasing amounts of protein decreased the size and increased the number density of domains of the lc phase. The radii of the domains decreased by nearly an order of magnitude for the 20 wt % film (Fig. 6 *D*). Prior to collapse, the film consisted of small solid domains surrounded by a network of bright

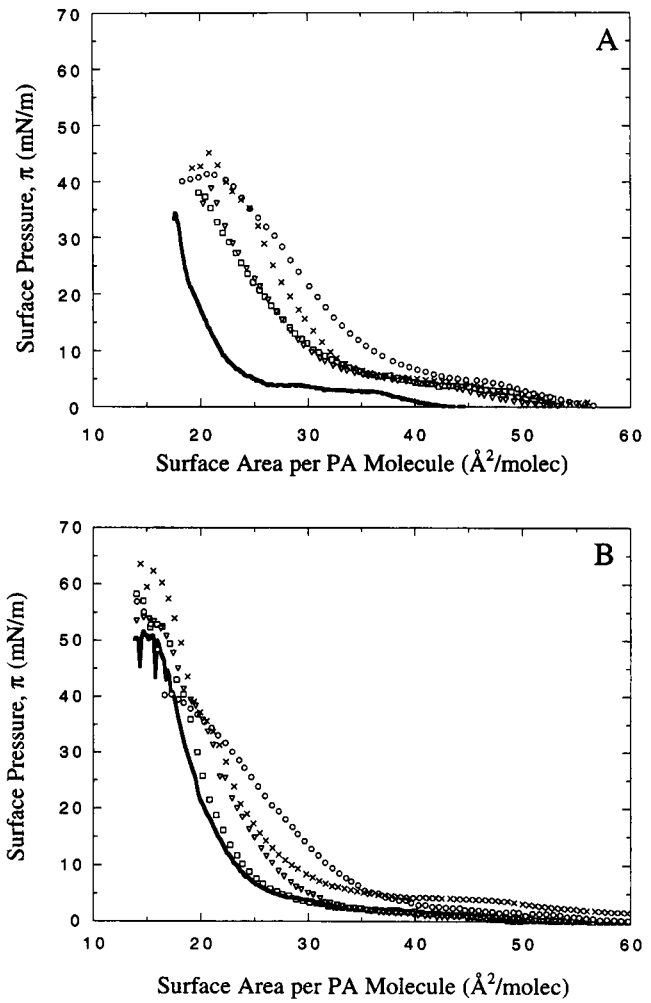

FIGURE 5 Surface pressure versus area per PA molecule isotherms as a function of peptide weight fraction. Isotherms of PA on (*A*) pure water (pH = 5.5) at 28°C and (*B*) buffered saline (0.15 M NaCl, pH = 6.9) at 25°C containing: 0 (—); 5 (□); 10 (▽); and 20 (○) wt % SP-B_{1-25}., and 20 (×) wt % SP-B_{1-78}.

phase, similar to the low temperature monolayers (Fig. 6 *E*). The presence of the protein resulted in a more homogenous collapse process; upon initiation of collapse, several nuclei appeared across the film. These nuclei grew into much smaller collapsed phase domains than in the absence of protein, and did not appear to be tilted when viewed via PFM (Fig. 6 *F*). These domains appeared to be less ordered and rigid than the domains seen in the pure PA film, and were incorporated back into the monolayer more readily upon expansion.

To determine the partitioning characteristics of the protein between the fluid and lc domains in Fig. 6, a dual probe experiment was conducted. A monolayer of PA and 20 wt % F-SP-B_{1-25} containing 0.5 mol % of Texas-red DPPE (which emits at a higher wavelength than fluorescein and has also been shown to partition into less-ordered phases) was prepared at 28°C on a pure water subphase. By quickly switching between filter cube assemblies specific for the emission wavelength of each of the fluorophores, the location of the tagged protein with respect to the bright fluid phase could be determined. On compression to the coexistence region, the tagged protein produced identical morphologies in the monolayer, as did the untagged protein. Images taken at the same locations throughout the coexistence region displayed the same morphology at both wavelengths (dark, circular domains in a bright background), a vivid demonstration that the protein partitioned into the disordered, fluid phase (Fig. 6, *G* and *H*). Images of a collapsed film showed that protein was also present to some extent in the growing and collapsed phase structures (Fig. 6 *I*).

PA/SP-B_{1-25} monolayers on a buffered saline subphase at 25°C

Results for the buffered saline subphase at 25°C (a few degrees above the triple point temperature of PA at these conditions) were qualitatively similar to the pure water case, with differences seeming to arise from the greater ionization of these films. Isotherms are shown in Fig. 5 *B*; again the collapse pressures were greatly increased for the physiological subphase. For pure PA monolayers, the amount of gas phase decreased on compression until a uniform le phase remained at the lift-off area of 48 Å²/mol. At a surface pressure of ~1.5 mN/m (area ~45 Å²/mol), dark lc domains nucleated from the le phase. The lc domains initially repelled each other, forming a hexagonal lattice with the domains avoiding contact (Fig. 7 *A*). At the end of the le-lc plateau region the pressure began to increase more sharply, corresponding to the initiation of close-packing and eventual contact of the lc domains. At this point, the lc domains fused with each other, forming a continuous network at a pressure of ~15 mN/m (Fig. 7 *B*). The remaining le subsequently disappeared, leaving a uniform sheet of condensed phase which persisted up to collapse of the monolayer at a pressure of ~52 mN/m. The buffered saline subphase conditions again resulted in a bulk fracturing mechanism for collapse of these pure PA films; bright cracks appeared at the collapse point and propagated across the film (Fig. 7 *C*).

The addition of protein again served to both fluidize and increase the collapse resistance of these films. The domain sizes at equivalent pressures decreased as a function of increasing protein concentration (Fig. 7, *D–F*). The condensed domains also eventually began to fuse as the area decreased, though the degree of fusion greatly decreased as the protein concentration was increased to 20 wt % (Fig. 7 *G*). At the higher protein concentrations, the bright phase persisted up to increasingly higher surface pressures, and the lc-solid kink point seen in the pure PA film turned into a plateau region that corresponded to the disappearance of the bulk bright phase from the interstitial regions. However, a network of bright phase persisted up to collapse (Fig. 7 *H*), and would immediately reappeared if the monolayer was expanded before collapse was allowed to occur (data not shown). The collapse pressure increased with protein con-

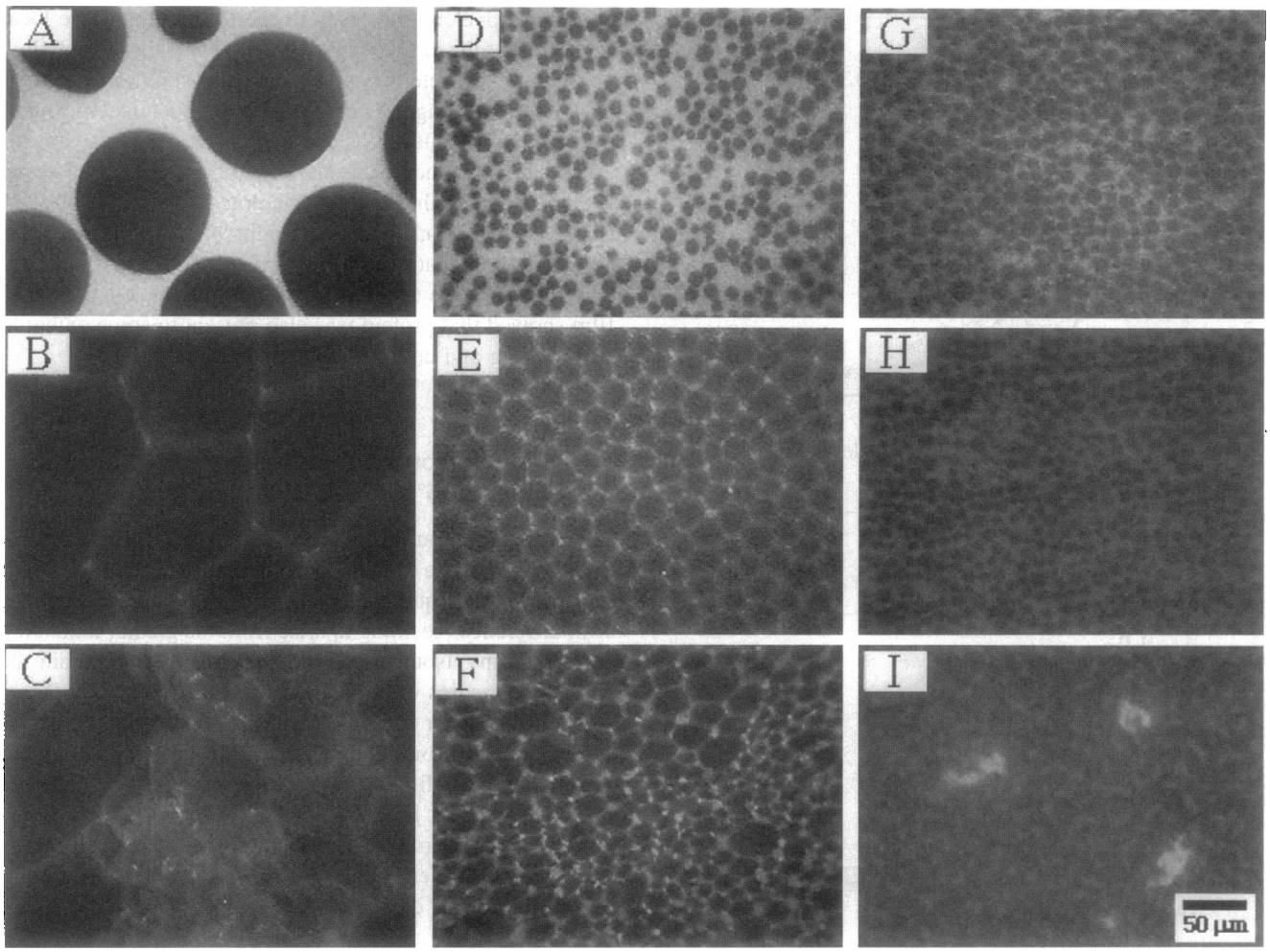

FIGURE 6 Images of PA and PA/SP-B_{1-25} films at 28°C on a pure water subphase. (*A–C*) Images of a pure PA film containing 0.5 mol % NBD-HDA. (*A*) Fluorescence image taken in the le-lc coexistence region. (*B*) Fluorescence image from the same film upon further compression into the solid phase. (*C*) Polarized fluorescence image taken postcollapse, showing the growth of a large domain of collapsed phase exhibiting tilt contrast. (*D–F*) Images of a PA/20 wt % SP-B_{1-25} film containing 0.5 mol % NBD-HDA. (*D, E*) Fluorescence images taken from (*D*) the fluid-lc coexistence region, and (*E*) immediately prior to collapse. (*F*) Polarized fluorescence image taken post-collapse, showing the nucleation and growth of small collapsed phase domains and a lack of-tilt contrast (the pattern of gray collapsed phase domains seen does not change upon rotation of the incident excitation beam). (*G–I*) Fluorescence images of PA/20 wt % fluorescein-SP-B_{1-25} films also containing 0.5 mol % Texas-Red DPPE showing (*G*) the fluorescence from the fluorescein and (*H*) Texas-Red fluorophores from the same region of a film in the fluid-lc coexistence region, and (*I*) the fluorescein emission at post-collapse of the film.

centration, reaching a value close to that for DPPC under the same experimental conditions. The mechanism for collapse again reverted to a homogeneous nucleation and growth process (Fig. 7 *I*), with small collapsed phase domains appearing uniformly across the monolayer.

Brewster angle microscopy of PA/SP-B_{1-25} films

BAM can be used to visualize PA/SP-B_{1-25} monolayers in order to confirm that the fluorescent probe does not influence the film morphology and phase transitions. As has been corroborated by many other studies comparing FM to BAM, the phase transitions and coexistence morphology seen with BAM were identical to those seen with FM, although the practical magnification achieved with BAM for our system was much less than that for FM (a field of view of width 8 mm for BAM compared to 400 μm for FM). This corroboration is particularly important for the collapse effects observed with FM, as monolayer collapse is a kinetic effect that occurs by a nucleation process and impurities in the monolayer can thus serve as nucleation sites for collapse. BAM images of similar films confirmed all major features observed with FM (decrease in domain size, increase in nucleation density, and homogeneous collapse in the presence of SP-B, etc.).

For the case of pure PA on a pure water subphase at 16°C, BAM images of the lc phase that appeared homogeneous with FM (see Fig. 3 *A*) revealed that at this temperature the lc phase is tilted (regions of different tilt orientation in Langmuir monolayers can be distinguished from regions of

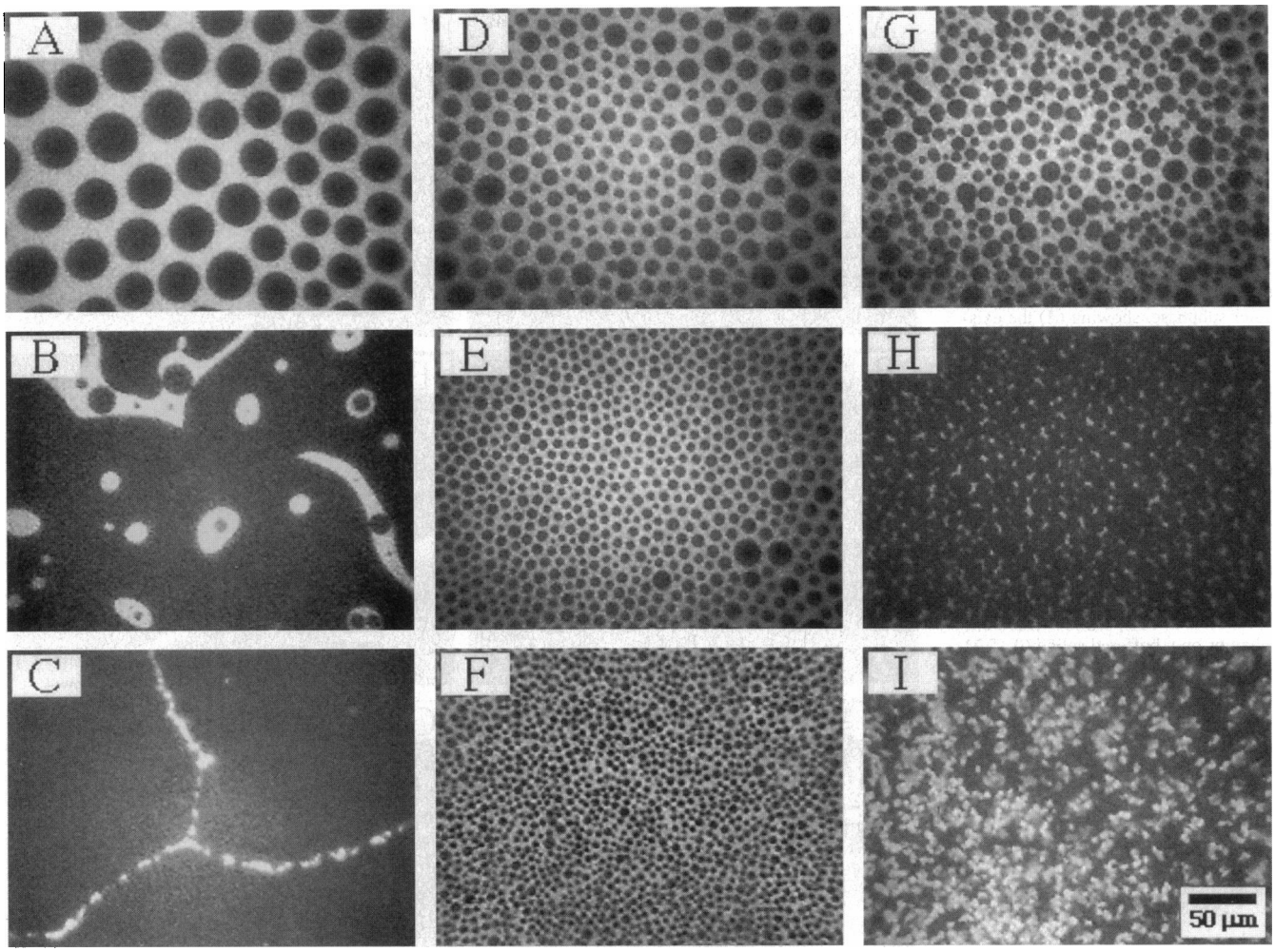

FIGURE 7 Images of PA/SP-$B_{1\text{-}25}$ films containing 0.5 mol % NBD-HDA on a buffered saline subphase at 25°C. (*A–C*) Images of a pure PA film in (*A*) the le-lc coexistence region, (*B*) after fusion of individual domains into a sheet of condensed phase upon further compression, and (*C*) the post-collapse fracturing of the film. (*D–F*) Images of a PA/SP-$B_{1\text{-}25}$ film in the le-lc coexistence region at an area per PA molecule of 35 $Å^2$ containing (*D*) 5, (*E*) 10, and (*F*) 20 wt % SP-$B_{1\text{-}25}$, showing the reduction in condensed domain size and increase in nucleation density with increasing protein concentration. (*G–I*) Images of a PA/20 wt % SP-$B_{1\text{-}25}$ film after (*G*) limited fusion of some condensed domains, (*H*) the same film immediately prior to collapse and (*I*) post-collapse, showing the nucleation and growth of small collapsed phase domains [in contrast to the fracturing process shown in (*C*)].

different phases via BAM by analyzing the polarization of the reflected light; by rotating a polarizer in the path of the reflected beam, regions of differing tilt direction will reverse their relative contrast upon rotation), as evidenced by a contrast resulting from regions of different tilt azimuth (Fig. 8 *A*). As shown by others (Bibo and Peterson, 1990; Moore et al., 1990; Schwartz and Knobler, 1993), the tilt is in the nearest-neighbor direction, making this phase an L_2 hexatic mesophase [or smectic I phase in the nomenclature of liquid-crystalline phases (Peterson, 1992)]. The tilt domains were of macroscopic dimensions; regions of constant tilt persisted over length scales on the order of millimeters in some cases (Fig. 8 *A*). On reaching the lc-solid transition (indicated by the high-pressure kink in Fig. 2 *A*), the contrast immediately disappeared from the entire film (Fig. 8 *B*), indicating the second-order nature of the transition from the tilted lc phase to the untilted solid phase. As observed with FM, collapse was again seen to proceed via a heterogeneous nucleation mechanism, with tilted collapsed phase domains nucleating with a low number density at various points across the film and growing into large, dendritic-type domains (eventually reaching dimensions on the order of millimeters). Upon addition of 20 wt % SP-$B_{1\text{-}25}$ at the same conditions, no tilt contrast was seen throughout the compression prior to collapse. This indicated that either the PA-rich lc domains were too small to be seen at these magnifications (consistent with the FM results) or that the protein partitioned into the condensed phases to some extent and perturbed the regular packing of the PA. Upon collapse of the monolayer, small nuclei appeared homogeneously across the film at a higher surface pressure than that of a pure PA film (Fig. 8 *E*). The eventual size of the individual collapsed domains remained very small (again consistent with the FM results), and the collapsed domains did not appear to be tilted (consistent with the PFM results, although the relatively low magnification limited a conclusive

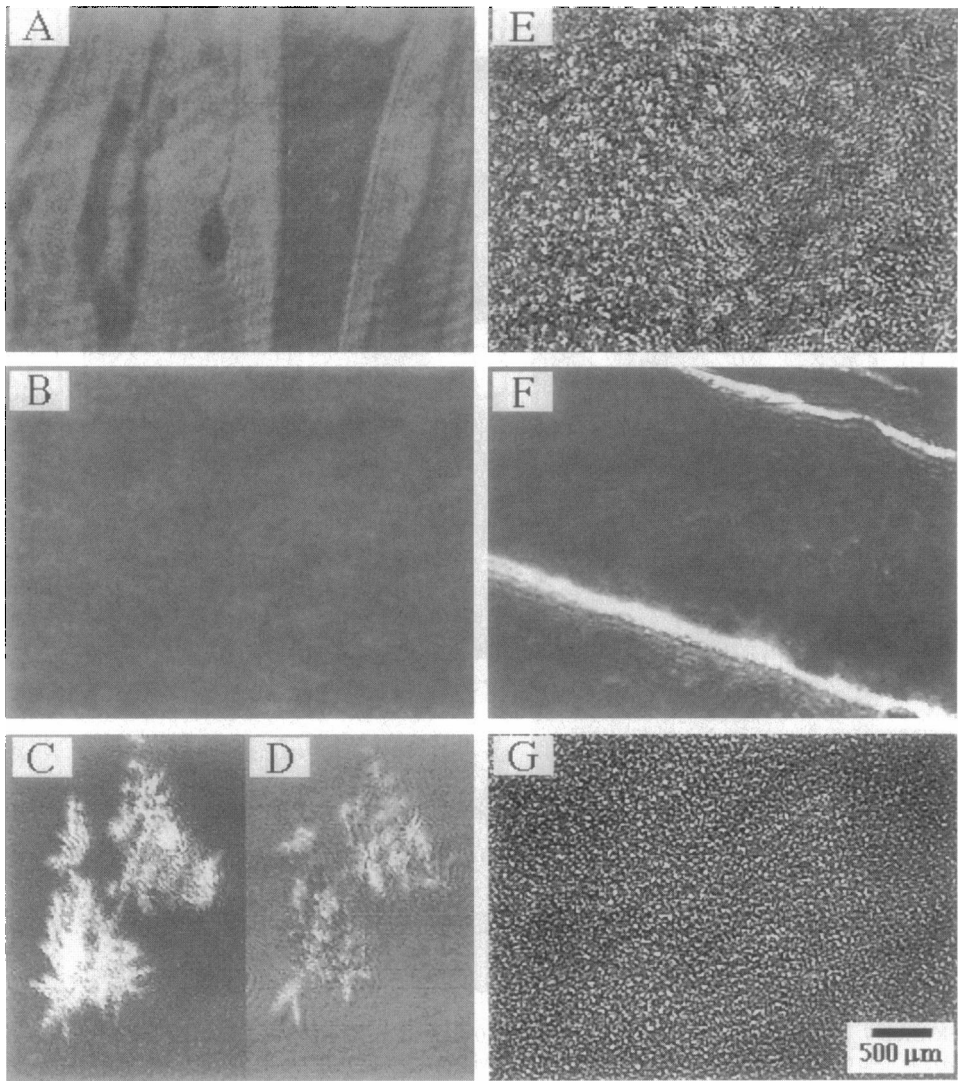

FIGURE 8 BAM images of PA and PA/SP-B films at 16°C. (*A–C*) Progression of a pure PA film on a pure water subphase, showing (*A*) the existence of different tilt domains in the pure lc phase, (*B*) the disappearance of the tilt contrast upon the transition into the solid phase, and (*C*, *D*) the formation of a tilted collapsed phase domains, with the analyzer rotated between images (*C*) and (*D*). (*E*) Collapse of a PA/20 wt % SP-B_{1-25} film on a pure water subphase showing the high nucleation density and limited growth of the collapsed phase domains. (*F*, *G*) Images of collapse behavior on a buffered saline (0.15 M NaCl, pH = 6.9) subphase, showing (*F*) the bulk fracture of a pure PA film upon collapse and (*G*) the formation of small collapsed phase domains at post-collapse of a PA/20 wt % SP-B_{1-25} film.

observation). The contrast in the collapse mechanism of these films on a buffered saline subphase at 16°C was clearly evident using BAM; the macroscopic dimensions of the fracture planes for a pure PA film can be seen in Fig. 8 *F*, while the homogeneous distribution of small collapsed phase domains occurring in a film containing 20 wt % SP-B_{1-25} can be seen in Fig. 8 *G*.

Similar trends were observed at temperatures above the triple point of PA on both pure water and buffered saline subphases (also in agreement with the FM and PFM data). For the case of pure PA on a pure water subphase at 28°C, the lc domains in coexistence with le phase appeared to be tilted (Fig. 9 *A*). Upon reaching the transition to the solid phase, the contrast disappeared across the film. Collapse also proceeded in a manner similar to the low-temperature case, with tilted dendritic domains nucleating and growing heterogeneously across the film (Fig. 9 *B* and *C*). For the 20 wt % SP-B film, the le-lc transition was not observable with BAM at these magnifications (consistent with the small size of the lc domains seen with FM). Collapse again proceeded in a homogeneous fashion at an elevated pressure, with no indication of tilt within the small collapsed phase domains (Fig. 9 *D*). Switching to a buffered saline subphase at 25°C, the fusion of lc domains and the bulk fracturing upon collapse of pure PA films seen with FM were also seen with BAM (Fig. 9 *E* and *F*). The shift to a more homogeneous nucleation and growth collapse mechanism in the presence of 20 wt % SP-B_{1-25} is shown in Fig. 9 *G*. Thus, BAM images of PA and PA/SP-B_{1-25} films fully agree with results obtained with FM and PFM, and at the same time provide additional information on the nature of the molecular packing in these films.

Comparison with full length SP-B_{1-78} synthetic protein

We have previously shown that SP-B_{1-25} possesses the same surface activity as the both the full-length sequence (SP-B_{1-78}) and native SP-B protein through isotherm data, surface activity and efficacy in animal models (Waring et al., 1989; Longo et al., 1993; Lipp et al., 1996). As shown below, this

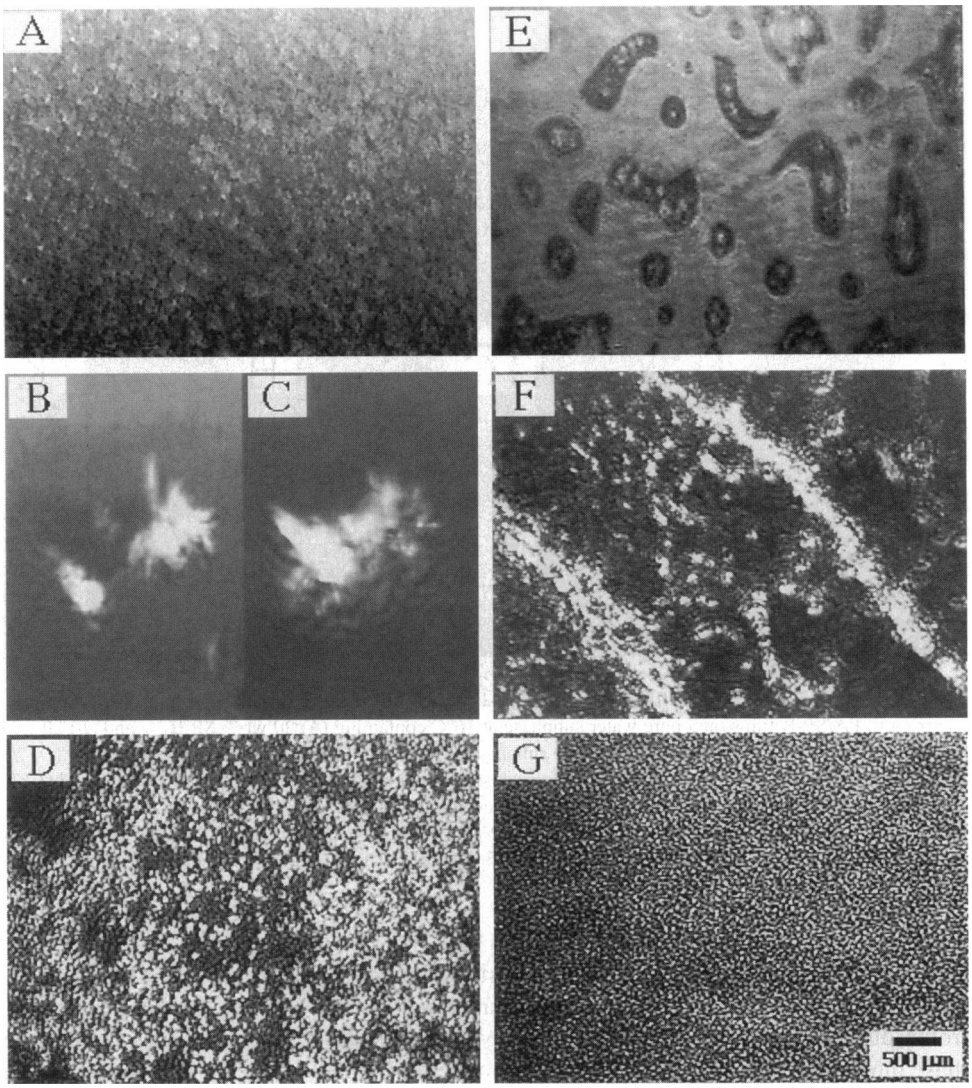

FIGURE 9 BAM images of PA and PA/SP-B_{1-25} films at temperatures above the triple point of PA. (*A–C*) Progression of a pure PA film on a pure water subphase at 28°C, showing (*A*) the film in the le-lc coexistence region, and (*B*, *C*) the same film post-collapse, with the tilt in the collapsed phase domain evident by the rotation of the analyzer between images (*B*) and (*C*). (*D*) Image of a PA/20 wt % SP-B_{1-25} film on a pure water subphase at 28°C, showing the growth of collapsed phase domains post-collapse. (*E–G*) Images of collapse behavior of PA and PA/SP-B_{1-25} films on a buffered saline (0.15 M NaCl, pH = 6.9) subphase at 25°C, showing (*E*) the fusion of the condensed phase domains in a pure PA film upon compression to elevated pressures prior to collapse, (*F*) the bulk fracturing of the same film upon collapse; and (*G*) the collapse behavior of a PA/20 wt % SP-B_{1-25} film, showing the nucleation and growth of collapsed phase domains.

similarity extends to the monolayer morphology as well. Results obtained using SP-B_{1-78} were completely analogous to those observed with SP-B_{1-25} at similar experimental conditions (with small differences appearing to arise from an increased surface viscosity due to the longer length of SP-B_{1-78}). Fig. 10 shows comparisons of PA films containing 20 wt % of either SP-B_{1-25} or SP-B_{1-78} at various experimental conditions and states of compression. Among the images shown are: collapse on a pure water subphase at 16°C of films containing (*A*) SP-B_{1-25} and (*B*) SP-B_{1-78}, the appearance of stripe phases in films on a buffered saline subphase at 16°C containing (*C*) SP-B_{1-25} and (*D*) SP-B_{1-78}, fluid-lc coexistence in films on a pure water subphase at 28°C containing (*E*) SP-B_{1-25} and (*F*) SP-B_{1-78}, collapse of these same films containing (*G*) SP-B_{1-25} and (*H*) SP-B_{1-78}, limited fusion of lc domains in films on a buffered saline subphase at 25°C containing (*I*) SP-B_{1-25} and (*J*) SP-B_{1-78}, and the collapse of these same films containing (*K*) SP-B_{1-25} and (*L*) SP-B_{1-78}. In all cases, the images are virtually identical. The major difference between the shortened peptide and the full-length protein is the greater insolubility in the subphase for the full-length protein, which may help to retain the protein in the monolayer.

Modified Gouy-Chapman analysis of the PA/SP-B_{1-25} system

The results obtained on the pure water and buffered saline subphases indicate that the monolayer electrostatics and the ionic strength of the subphase have a significant effect on the morphology and phase behavior of these films. Considering pure PA monolayers, switching from a pure water to a buffered saline subphase results in a drastic alteration in the monolayer collapse process from the heterogeneous nucleation and growth of large tilted crystalline phases at low pressures to a bulk fracturing process at higher pressures. For both cases, the presence of the protein in the monolayer results in an increase in the collapse pressure of the same order of magnitude (15 mN/m), and a shift to a more reversible homogeneous nucleation and growth process. To qualitatively explain these effects, the state of

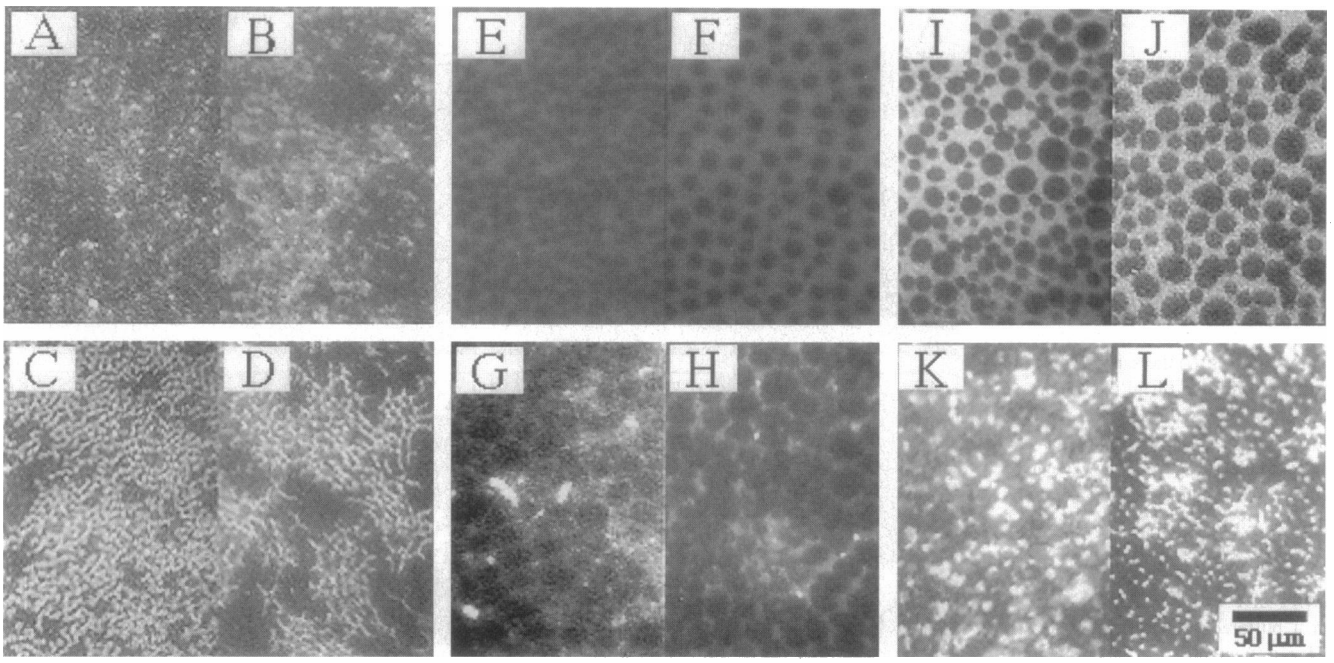

FIGURE 10 Comparison of PA films containing SP-B_{1-25} and SP-B_{1-78} at various experimental conditions. (*A*, *B*) Images of collapsed phase domains occurring in PA/SP-B films on a pure water subphase at 16°C containing (*A*) 20 wt % SP-B_{1-25} and (*B*) 20 wt % SP-B_{1-78}. (*C*, *D*) Images of stripe phases occurring in PA/SP-B films on a buffered saline subphase at 16°C containing (*C*) 20 wt % SP-B_{1-25} and (*D*) 20 wt % SP-B_{1-78}. (*E*, *F*) Images of PA/SP-B films on a pure water subphase at 28°C in the le-lc coexistence region containing (*E*) 20 wt % SP-B_{1-25} and (*F*) 20 wt % SP-B_{1-78}. (*G*, *H*) Images of PA/SP-B films on a pure water subphase at 28°C post-collapse containing (*G*) 20 wt % SP-B_{1-25} and (*H*) 20 wt % SP-B_{1-78}. (*I*, *J*) Images of limited fusion of lc domains PA/SP-B films on a buffered saline (0.15 M NaCl, pH = 6.9) subphase at 25°C in the le-lc coexistence region containing (*I*) 20 wt % SP-B_{1-25} and (*J*) 20 wt % SP-B_{1-78}. (*K*, *L*) Images of PA/SP-B films post-collapse on a buffered saline (0.15 M NaCl, pH = 6.9) subphase at 25°C containing (*K*) 20 wt % SP-B_{1-25} and (*L*) 20 wt % SP-B_{1-78}.

charge at the interface and the electrolyte distribution in the subphase must be estimated. A common approach for a proton-dissociable surfactant at an air/monovalent salt subphase interface is to combine Gouy-Chapman theory with a simple mass action expression to allow for the dissociation of the molecules in the monolayer (Helm et al., 1986). For such systems, the GC model predicts the extent of dissociation and surface charge density of the monolayer, as well as the subphase concentration profile adjacent to the monolayer. The region that the concentration varies with respect to the bulk phase concentration can be estimated by calculating the Debye length of the system; the concentrations of the individual ions in the subphase reach their bulk values approximately a Debye length away from the surface.

GC analysis of a monolayer assumes a homogeneous composition and lateral density distribution. As seen in the fluorescence images presented in the previous sections, both the composition and density can vary over a range of length scales, depending on the overall composition of the monolayer (pure PA versus PA/SP-B_{1-25}) and the overall area per molecule at a given point of the isotherm. Thus, any attempt to use the GC model in this case must be done within the individual homogeneous phase domains. However, the characteristic length scale of the domains observed in the images presented in this paper are on the order of microns, while the characteristic length scale of the GC analysis, which is the Debye length, is on the order of nanometers. Hence, the GC analysis should be valid within any given domain. An additional complication is that the lateral density, and thus the area per molecule, is different in each of the coexisting phases during phase transitions. However, a good estimate of the area per molecule within each phase can be obtained from the overall area per molecule at the endpoints of the transition region.

For the qualitative comparisons needed here, there are three limiting composition regimes: areas of essentially pure PA, areas of complete mixing (based on the overall composition), and areas enriched in protein. For areas of pure PA, literature results for homogeneous fatty acid monolayers can be used to predict the local extent of dissociation and subphase ionic distribution (Helm et al., 1986). For the completely mixed regions, the positively charged protein must be accounted for when calculating the local surface charge density. Finally, for the protein-rich regions, both the area per protein molecule and the amount of PA present must be estimated. Two limits within this protein-rich regime may be considered: 1) a 4:1 PA/SP-B_{1-25} ratio based on charge neutralization, and 2) pure protein. The results for these limiting cases give a good estimate of the local surface charge density, extent of PA dissociation, and pH, and provide a qualitative explanation of the alterations in both condensed phase nucleation density and size and the monolayer collapse pressure on pure water and buffered saline subphases.

For regions composed primarily of PA, the equilibrium reaction under consideration is (in addition to the dissociation of water)

$$[H^+]_s + [L^-] \leftrightarrow [HL], \quad K_L \tag{1}$$

where $[H^+]_s$ is the concentration of protons in the vicinity of the surface, $[L^-]$ is the surface concentration of ionized lipid, [HL] is the surface concentrations of protonated lipid, and K_L is the association constant for the lipid. Combining this mass-action equation with the GC equations for a homogeneous, single-component monolayer results in an expression for the surface charge density via the solution of a set of transcendental equations of the form (Helm et al., 1986)

$$\sigma = \left\{2\varepsilon\varepsilon_o k_B T \sum_i c_{i,b}(\exp[-q_i\psi_o/k_bT] - 1)\right\}^{1/2} \tag{2}$$

$$\sigma = \frac{e/A}{1 + K_L[H^+]_b \exp[-e\psi_o/k_BT]}, \tag{3}$$

where σ is the surface charge density, ε is the dielectric constant in the vicinity of the interface, ε_o is the permeability of vacuum, k_B is Boltzmann's constant, T is temperature, c_i and q_i are the number density and charge of the ionic species i, respectively (b denotes a bulk subphase concentration); ψ_o is the surface potential; e is the unit charge; and A is the area per molecule. Equation 3 was obtained from the definition of the extent of the dissociation of the monolayer, α, given that

$$\alpha = \frac{[L^-]}{[L^-] + [HL]}, \tag{4}$$

and noting that $\sigma = (e/A)\alpha$.

For buffered saline subphases, it is assumed that the subphase pH remains constant at the buffered value, and the contribution of the buffer to the ionic strength of the subphase is negligible with respect to the salt concentration. The addition of salt leads to two additional equilibrium equations of the form

$$[M^+] + [X^-] \leftarrow [MX], \quad K_{MX}(=0) \tag{5}$$

$$[M^+]_s + [L^-] \leftrightarrow [ML], \quad K_M \tag{6}$$

where $[M^+]$ and $[X^-]$ are the concentrations of salt cations and anions, respectively (and also assuming complete dissociation, i.e., $[MX] = K_{MX} = 0$), and K_M is the association constant for lipid with bound cation. For this case, the salt ion concentration is simply factored into Eq. 2, and Eq. 3 becomes

$$\sigma = \frac{e/A}{1 + \{K_L[H^+] + K_M[M^+]\}\exp[-e\psi_o/k_BT]} \tag{7}$$

To extend this theory for regions of complete mixing in the PA/SP-$B_{1\text{-}25}$ films, the charged protein must be accounted for. A generalized schematic of the protein-containing system displaying the relevant parameters is shown in Fig 11. For the pure water subphase, Eqs. 5 and 6 can be neglected. The protein is added initially in neutral form with four equivalent anions per molecule (for charge compensation, most likely chloride ions retained from the lyophilization solvent). The number of moles added is denoted as $[PX_4]_{ic}$, and this addition results in a contribution of $4[PX_4]_{ic}$ moles of anions to the ionic strength of the subphase upon dissociation. The presence of the protein thus leads to an additional equilibrium equation of the form

$$[P^{4+}] + 4[L^-] \rightarrow [PL_4], \quad K_P, \tag{8}$$

where $[P^{4+}]$ is the surface concentration of added protein, $[PL_4]$ is the surface concentration of lipid-associated protein (assuming their binding stochiometry is dictated by the protein's net positive four charge), and K_P is the association constant for the reaction. Under these conditions, Eq. 4 becomes

$$\alpha = \frac{[L^-]}{[L^-] + [HL] + 4[PL_4]}. \tag{9}$$

We also assume that all of the added protein remains in the monolayer and associated with lipid (i.e., $K_p \gg 1$), so that $[PL_4] = [PX_4]_{ic}$. When these equilibrium concentrations are plugged in, Eq. 1 becomes

$$K_L = \frac{B - [L^-]}{[L^-][H^+]_s} \tag{10}$$

where B is equal to $\{[HL]_{ic} - 4[PX_4]_{ic}\}$ and $[HL]_{ic}$ is the amount of lipid added. Inserting these results into the dis-

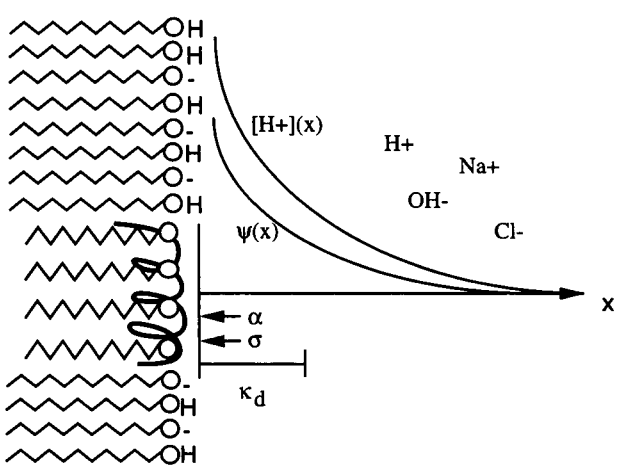

FIGURE 11 A schematic representing the model used for the Gouy-Chapman analysis of the PA/SP-$B_{1\text{-}25}$ system. A PA/SP-$B_{1\text{-}25}$ monolayer is depicted with a coexistence between condensed PA domains and a PA/SP-$B_{1\text{-}25}$-complexed fluid domain (with the protein denoted by the helical line segment). The x coordinate is normal to the monolayer. $[H+](x)$ and $\psi(x)$ are the proton concentration and electrostatic potential as a function of distance from the interface, respectively. α and σ are the extent of dissociation at the surface and the surface charge density, respectively. κ_d is the system Debye length. The relevant salt, proton, and hydroxide counterions are also shown.

sociation equation for the lipid-protein film and rearranging yields

$$\sigma = \frac{e/A}{\left(1 + \left(\frac{4}{B}\right)[PX_4]_{ic}\right)(1 + K_L[H^+]_b \exp[-e\psi_o/k_BT])} \quad (11)$$

where $[H^+]_s$ has been related to the bulk proton concentration $[H^+]_b$ via the Boltzmann relation. This equation will then be solved simultaneously with Eq. 2. To extend this case to a buffered saline subphase, if it is assumed that sodium cations do not bind to the lipid headgroups, then Eq. 11 will remain unchanged, while the concentration of added salt will again be factored into Eq. 2. This system of equations can be further simplified by noting that the addition of 0.15 M NaCl dominates the contribution of counterions from the fatty acid, protein, and pH buffer. In this case, Eq. 2 can be simplified for the case of a symmetric 1:1 electrolyte, which yields

$$\sigma = \left(\frac{2\varepsilon_o \varepsilon \kappa_d k_B T}{e}\right) \sinh\left(\frac{e\psi_o}{2k_BT}\right) \quad (12)$$

where κ_d^{-1} is the Debye length, given by

$$\kappa_d^{-1} = \sqrt{\frac{\varepsilon_o \varepsilon k_B T}{q_i^2 \sum c_{i,b}}} \quad (13)$$

If the increase in pH and subphase ionic strength leads to a relatively high surface potential with respect to thermal energy, then $\sinh(x) \sim 1/2 \exp(x)$, giving rise to

$$\psi_o = \left(\frac{2k_BT}{e}\right) \ln\left(\frac{\sigma e}{\varepsilon_o \varepsilon \kappa_d k_B T}\right) \quad (14)$$

Plugging this into Eq. 11 gives

$$\sigma = \frac{e/A}{\left(1 + \left(\frac{4}{B}\right)(PX_4)_{ic}\right)\left(1 + K_L[H^+]_b \left\{\frac{\sigma e}{\varepsilon_o \varepsilon \kappa s_d k_B T}\right\}^{-2}\right)} \quad (15)$$

which can then be solved iteratively to give the surface charge density. This simplified form for buffered saline subphases can also be used for the PA-rich regions (in lieu of Eqs. 2 and 3) by setting $[PX_4]_{ic}$ equal to zero.

For the protein-rich regions, the limiting case of stochiometric binding of dissociated PA and SP-$B_{1\text{-}25}$ in a 4:1 ratio will give a net surface charge density of zero. For this situation, the ionic concentrations at the interface will be the same as their bulk values. Considering the limiting case of regions of pure protein, the high pI of SP-$B_{1\text{-}25}$ (~10.4) with respect to the bulk pH for both pure water and buffered saline subphases will result in full protonation of the four basic residues of the protein. For this case, the surface charge density will simply be determined by the area per molecule of the protein, and the surface pH can be obtained for both the pure water and buffered saline cases by solving for the surface potential in Eq. 2.

The above analysis was applied at selected conditions to relate the electrostatic state of the interface and surrounding subphase to the observed monolayer morphologies and phase transitions. All equations were solved numerically via Mathematica. For the case of monolayer collapse, the analysis was applied to both pure and protein-containing PA monolayers on both pure water and buffered saline subphases. As evidenced by the results in Table 1, the ionic state in the interfacial region is very different for each subphase, and helps to explain the different collapse processes occurring in pure PA films. Equations 2 and 3 were solved for the case of a pure PA monolayer on a pure water subphase, and Eqs 2 and 8 for a buffered saline subphase; a literature pK value of 5.4 for PA (Cockshutt et al., 1991), a subphase temperature of 16°C and an area per PA molecule of 17 Å^2 were used in both cases. For the pure water conditions, the absence of salt counterions results in a low surface pH (2.8) and low extent of dissociation (0.002). The increased ionic strength of the buffered saline subphase results in a significant increase in the surface pH (4.9) and extent of dissociation (0.24), which leads to a relatively high surface charge density for the monolayer (0.22 C/m^2). This increase in surface charge density and ionization correlates with the shift in the observed collapse mechanism from growth of large collapsed phase domains at a low supersaturation pressure (40 mN/m) on pure water to a fracturing process at a higher pressure (55 mN/m) on a buffered saline subphase. The high surface charge density for the buffered saline subphase prevents the formation of bulk collapse structures, most likely due to the electrostatic repulsion that would exist in these structures upon exposure of the ionized PA molecules to the region of low dielectric constant above the monolayer.

For the protein-containing films, the bright phase network diminishes in width but still appears to persist up to collapse, separating and partitioning the circular condensed domains. The average radii of these domains on both pure water and buffered saline subphases at 16°C were on the order of 5–10 μm. Collapse seemed to occur primarily inside these domains on both subphases. The domains also appeared to consist primarily of PA, as evidenced from the lack of fluorescence intensity within these domains for films containing F-SP-$B_{1\text{-}25}$. The Debye lengths calculated for the

TABLE 1 Results of the Gouy-Chapman model for the electrostatic conditions at collapse for PA and PA/20 wt % SP-$B_{1\text{-}25}$ monolayers below the triple point

	Pure water subphase	Buffered saline subphase
Area/molecule (Å^2)	17.0	17.0
Temperature (°C)	16.0	16.0
Salt conc. (M)	0.0	0.15
Bulk pH	5.5	6.9
Debye Length (nm)	241	0.78
Surface pH	2.8	4.9
Dissociation extent	0.002	0.24
Surface charge (C/m^2)	0.002	0.22

pure PA films at collapse on pure water and buffered saline subphases are 241 and 0.78 nm, respectively (Table 1). Since both of these values are much lower than the average radii of the condensed domains for both subphase conditions, the GC analysis should hold within the individual domains. This means that the electrostatic conditions within the domains are the same at collapse as in the absence of protein. However, as the addition of protein results in an increase in the collapse pressure of ~15 mN/m for both subphases, this result indicates that the protein raises the collapse pressure via an effect other than a simple electrostatic-based interaction within the domains. This provides evidence that the partitioning effect of the protein network is primarily responsible for the higher collapse pressures.

For pure water and buffered saline subphases, both in the presence and absence of protein, monolayers of PA at temperatures above their triple point pass through a homogeneous fluid phase before condensed phases are formed. The GC analysis can also be used to describe the electrostatic state of these homogeneous fluid phases during nucleation of condensed phases. For pure PA, switching from a pure water to a buffered saline subphase increases the nucleation density by an order of magnitude, and decreases the size of the condensed phase domains at similar phase area fractions (Table 2). Using an area per PA molecule of 40 $Å^2$ for the initiation of the expanded-to-condensed transition for both cases, the surface pH increases from 3.1 to 5.2 and the extent of dissociation increases from 0.004 to 0.39 upon switching to a buffered saline subphase (Table 2). This significantly increases the surface charge density, which increases the electrostatic repulsion within the critical lc nuclei. Domain shapes at a particular point of compression of a monolayer usually result from a balance between electrostatic repulsion and line tension; electrostatic repulsion favors the elongation of domains of the more condensed phase due to their higher lateral density, while line tension favors circular domains that minimize the interphase perimeter. This balance most likely also has an influence on the size of the nuclei in monolayers undergoing a phase transition. Assuming the line tension remains unchanged, the increased electrostatic density in charged monolayers results in a smaller critical radius for the nuclei (with a corresponding increase in the required supersaturation pressure), which would account for the observed increase in nucleation density.

However, for both pure water and buffered saline subphases at temperatures above the triple point for pure PA, the presence of protein results in a drastic increase in the nucleation density and a decrease in the lc domain sizes over those for pure PA at the same conditions (see Table 2). Assuming that the condensed domain nuclei do not contain protein and that the protein does not act as a heterogeneous site for nucleation (which is consistent with the observed experimental results), then the protein will influence the nucleation process only through its effects on the surrounding fluid phase. The protein in the low weight percentages used has little effect on the electrostatic conditions of the homogeneous fluid phase at the fluid-to-condensed transition point (Table 2). From solving Eqs. 2 and 11, the calculated values of the surface pH and extent of dissociation change only slightly; for pure a water subphase the surface pH is 3.1 and the extent of dissociation is 0.005, for buffered saline the surface pH is 5.3, and the extent of dissociation is 0.4. Thus, assuming that the nucleation density is dictated by the balance of electrostatic repulsion and line tension forces of the critical nuclei, the protein appears to lower the line tension between the fluid and condensed phases. This lowered line tension is manifested by the appearance of increased perimeter between the condensed and expanded phases, which persists to high pressures and allows for the formation of the bright phase network up to collapse. As shown in Table 2, the average condensed phase domain radii for PA/20 wt % SP-B_{1-25} films on both pure water and buffered saline subphases remain on the order of microns up to high pressures, which results in a high amount of perimeter between the condensed and fluid phases.

This alteration in the balance between line tension and electrostatic forces is also evidenced by the appearance of

TABLE 2 Results of the Gouy-Chapman model and image analysis for the expanded-to-condensed phase transition for PA and PA/20 wt % SP-B_{1-25} monolayers above the triple point

	Pure PA/Pure water	Pure PA/Buffered saline	PA/20 % SP-B_{1-25}/ Pure water	PA/20 % SP-B_{1-25}/ Buffered saline
Area/molecule ($Å^2$)	40	40	45	45
Temperature (°C)	28	25	28	25
Salt conc. (M)	0.0	0.15	0.0	0.15
Bulk pH	5.5	6.9	5.5	6.9
Debye Length (nm)	245	0.79	245	0.79
Surface pH	3.1	5.2	3.1	5.3
Dissociation extent	0.004	0.39	0.005	0.40
Surface charge (C/m^2)	0.002	0.16	0.002	0.14
Nucleation density (mm^{-2})	50	970	4400	9700
Avg. domain radius (μm) at π = 30 mN/m	—	—	10	8
Perimeter/area (mm^{-1}) at π = 30 mN/m	—	—	280	220

The Gouy-Chapman parameters and the nucleation density were calculated at the initiation of the transition, and the average domain radii and perimeter per area were calculated at a surface pressure of 30 mN/m.

stripe phases on buffered saline subphases at low temperatures for PA/20 wt % SP-B films. McConnell et al. have shown that the equilibrium width of a stripe is proportional to $\exp(\lambda/\mu^2)$, where λ is the effective line tension between domains, and μ is the difference in dipole density between the phases (McConnell, 1989). Taking an area per molecule of 60 Å^2 (the approximate area per molecule at which stripe phases were observed) for the solution of Eqs. 2 and 3, any PA-rich regions will possess an extent of dissociation of 0.48 and a surface charge density of 0.12 C/m^2. Protein-rich phases will either be neutral if associated with PA or will possess a net positive charge, which will lead to a large charge density difference between the two phases. If the line tension between two such phases is sufficiently small, this could drive the formation of stripe phases. Stripe phases are also observed in pure films of F-SP-$B_{1\text{-}25}$. The co-existence of protein domains of differing density could result in a dipole difference between the phases. Using an area per F-SP-$B_{1\text{-}25}$ molecule of 300 Å^2 (which is approximately the lift-off area for pure F-SP-$B_{1\text{-}25}$ films, data not shown), the surface charge density will be ~0.15 C/m^2; if the line tension between the gaseous and condensed protein phases is low enough, this could also result in the appearance of stripes.

DISCUSSION

SP-B has been hypothesized to fulfill a number of essential roles in the LS system, including the transport, interconversion, and spreading of monolayers from lung multilamellar bodies, as well as the optimization of surface activity of the monolayer itself (Fleming and Keough, 1988; Cochrane and Revak, 1991; Shiffer et al., 1993). An unresolved issue concerning the surface activity of LS is the fate at high surface pressures of the anionic lipids and fatty acids that act as fluidizing components. The relatively low collapse pressures of these components has led to the belief that they are "squeezed out" of the monolayer, leaving behind a monolayer enriched in DPPC (Cockshutt et al., 1991; Pastrana-Rios et al., 1994). However, the improved respreadability of natural lung surfactant after collapse in comparison to DPPC, and the fast dynamics of the breathing cycle, makes this hypothesis difficult to believe. These squeeze-out hypotheses typically neglect the influence of proteins on the monolayer behavior or claim that the proteins facilitate the selective removal of fluidizing components from LS monolayers (Pastrana-Rios et al., 1994; Taneva and Keough, 1994). An alternative theory for the role of proteins in LS is that they serve to further increase the fluidity of LS while retaining the anionic lipid components in the monolayer, thus allowing for low surface tensions in the mixed monolayer while providing for a more respreadable collapsed phase. Such a synergistic interaction between the proteins and fluidizing lipids would be primarily electrostatic in nature, as evidenced by the effects we have shown by varying the subphase pH and ionic strength, as well as the failure of an uncharged mutant form of SP-B to either interact with PA monolayers at high surface pressures or to increase their surface activity (Waring et al., 1989; Cochrane et al., 1991; Longo et al., 1993). Thus, a detailed knowledge of the influence of LS proteins such as SP-B on the surface behavior of anionic lipids could reveal the function of these proteins in the LS monolayer.

The addition of either SP-$B_{1\text{-}25}$ or SP-$B_{1\text{-}78}$ has two main effects on the phase behavior of PA monolayers: 1) the monolayers are fluidized and 2) collapse is shifted to a reversible, high-pressure nucleation and growth-type event. The fluidization induced by the protein inhibits the formation of condensed phases, decreasing the average size and increasing the density of the condensed phase domains. The protein partitions preferentially into the disordered fluid phase, which persists to high pressures and forms a network partitioning and segregating the condensed phase domains prior to collapse. The small size of the condensed phase domains results in a large amount of perimeter between the protein-rich network phase and the condensed phase. Upon collapse, small collapsed phase domains nucleate and grow homogeneously across the monolayer, and reincorporate reversibly into the monolayer upon expansion.

It appears that the formation of the protein network is the key to both the increase in fluidity and the shift in the collapse mechanism of PA monolayers. The fluidity and collapse behavior of fatty acid monolayers can be modulated by altering the pH and ionic strength of the subphase; this modulation is well-described by traditional Gouy-Chapman electrostatic theory (Helm et al., 1986; Lösche and Möhwald, 1989; Pezron et al., 1990). Fatty acid monolayers on suphases at low pH and monovalent salt concentration exist in an un-ionized state; these monolayers are condensed at temperatures below their triple point and collapse irreversibly at relatively low pressures by the formation of large, rigid multilayer collapsed phase domains. Increasing the subphase pH or monovalent salt concentration serves to ionize these monolayers, effectively lowering their triple point temperature and shifting the collapse mechanism to a higher-pressure, irreversible, bulk-fracturing event. The addition of monovalent or divalent salts in concentrations high enough to induce binding to the monolayer serve to condense ionized monolayers and in some cases can stabilize them further against collapsing; however, collapse still occurs irreversibly.

In contrast, on both pure water and buffered saline subphases, SP-B protein both fluidizes PA monolayers and increases their collapse pressure by ~15 mN/m, shifting the collapse mechanism to a more homogeneous and reversible event. The failure of the Gouy-Chapman theory (with the presence of the protein accounted for) to account for this behavior indicates that the collapse mechanism shift is a direct effect of the partitioning of the condensed phase domains by the protein-rich network in lieu of a simple charge counterion effect. Additionally, it appears that for the network to function properly, the average condensed domain size must be small. This necessitates a large amount

of perimeter between the network and the condensed phase domains. The observation of increased nucleation densities of condensed phases and the formation of stripe phases in the presence of protein indicate that the balance of charge density to line tension between the condensed and protein-rich phases has been altered. The modified Gouy-Chapman analysis indicates that this alteration is primarily due to a low-line tension between the condensed and protein-rich phases. It is this lowered line tension that facilitates the increase in perimeter between the condensed phase domains and the protein-rich network.

These observations can be combined to provide a model linking the molecular interactions between PA and SP-B in the monolayer to the surface morphology and properties of the monolayer, and their implications on the function of these components in the complete lung surfactant monolayer. This model contains three basic features: 1) The addition of protein induces the formation of a fluid, protein-rich phase in the PA monolayer and increases its compressibility; 2) a low-line tension allows for significant amounts of a protein-rich network to form around the condensed phase domains; 3) the presence of this network breaks up and partitions the condensed phase domains, converting the collapse mechanism from heterogeneous, large length scale processes to a homogeneous, high-pressure process that provides for more reversible respreading of the collapsed monolayer.

Fluidization and lowered line tension of PA monolayers by SP-B

The effect of SP-$B_{1\text{-}25}$ on the fluidity of PA monolayers is apparent under all experimental conditions. Below its triple point temperature, PA transforms into an incompressible liquid-condensed phase via reverse sublimation from the gas phase upon compression. The addition of increasing amounts of SP-$B_{1\text{-}25}$ to PA monolayers at 16°C on both pure water and saline subphases creates a fluid phase, increasing the compressibility of the monolayer and inhibiting the formation of an extended lc phase. That the fluid phase is protein-rich is confirmed by several observations. At equivalent surface pressures, the percentage of fluid phase increases as a function of increasing protein concentration. The brightness of this fluid phase also suggests the presence of the protein. The probe used in this study prefers to partition into the less-ordered phases in monolayers, making these phases appear brighter than the more condensed phases (Knobler, 1990). As the protein serves to inhibit the close-packing of PA hydrocarbon chains, and hence disorders the system, the probe therefore prefers to sequester in its vicinity. Also, the hydrophobic environment of the protein serves to shield the fluorophore from the water and increase its quantum yield. Finally, the use of fluorescein-labeled SP-$B_{1\text{-}25}$ positively identifies the bright phase as protein-rich in PA/F-SP-$B_{1\text{-}25}$ films. The fluid phase persists after liftoff and appears to be in equilibrium with the more condensed phase throughout the pressure regime, which corresponds to the homogeneous lc phase in the pure PA monolayer. This fluid phase reversibly shrinks and grows as the monolayer is compressed and expanded throughout an isotherm cycle, which indicates that this phase remains in the monolayer instead of being selectively removed into the subphase.

Raising the temperature above the triple point for PA on both subphases has a significant effect on the fluidity of the films. The protein alters the nucleation of condensed phases, resulting in smaller lc domains with a higher nucleation density. Nucleation in monolayers at a phase transition is usually an activated process, with the number and initial size of domains being determined by a competition between the favorable decrease in free energy due to the condensation process balanced by the unfavorable increase in free energy due to interfacial energy and electrostatic repulsion of the headgroups within the condensed phase. If the presence of the protein leads to a low-line tension between the condensed and fluid phases, which is supported by the results of the GC calculations and the observed increases in condensed phase nucleation density and interphase perimeter, this can lead to smaller critical radii for the nucleating domains and result in higher nucleation densities.

The presence of stripe phases at high protein concentrations under certain experimental conditions also indicates that the line tension has been lowered. Stripe phases have been observed in a variety of different physical systems, and are usually due to the presence of competing forces (Seul and Andelman, 1995). In Langmuir monolayers, stripe phases typically arise when the electric dipole density difference between coexisting domains overwhelms the line tension, thus elongating the domains. We have observed stripe phases both in mixed PA/SP-B films and in pure fluorescein-SP-$B_{1\text{-}25}$ films. The presence of stripe phase in the pure fluorescein-SP-$B_{1\text{-}25}$ film implies that the phenomena is intrinsic to the protein. For the mixed PA/SP-$B_{1\text{-}25}$ films, the fact that stripes are observed only under buffered saline subphase conditions, for which the electrostatic repulsion between headgroups is higher due to their higher degree of ionization, indicates the delicate nature of this balance. The net result of a lowered line tension (whether it leads to the formation of a stripe phase or not) is the presence of a greater amount of interphase perimeter in the system at equilibrium, which appears to have drastic consequences on the mechanism of collapse for these monolayers.

Influence of SP-B on the collapse and respreading of PA monolayers

SP-$B_{1\text{-}25}$ has a significant effect on the collapse resistance of PA monolayers. This effect appears to be electrostatically facilitated due to the opposite charges of the protein and the PA molecules (and a loss of activity when removing the protein's positive charge, data not shown), but appears to occur via a more specific mechanism than simple electro-

static screening or ionic binding. No theories yet exist that can accurately predict the nature of collapse of surfactant monolayers at the air-water interface under all experimental conditions. Several models have been developed for the collapse of single chain lipids, such as fatty acids, based on the assumption that collapse proceeds via a homogeneous nucleation and growth mechanism and that the collapse pressure can be predicted from classic nucleation theory applied to a two-dimensional system (Smith and Berg, 1980; De Keyser and Joos, 1984; Pezron et al., 1990). However, such theories assume that the monolayer is energetically uniform in its entirety, which may not be the case. Although the presence of dust does not appear to facilitate nucleation of collapse, other surface-active impurities in the monolayer could very well act as favorable sites for nucleation of collapse. Additionally, PFM and BAM images show that the lc phase in PA monolayers actuality consists of a polycrystalline-like array of domains of differing tilt direction, bordering each other at disinclination lines and points. Although the lc phase is transformed into an untilted solid phase prior to collapse in these monolayers, compression at significant rates may not allow for the annealing of the disinclination lines and points in the transformed solid phase; these heterogeneous sites can lower the activation energy for nucleation of collapsed phases.

A bulk fracturing process can supersede the nucleation of collapse domains in lipid films under certain conditions. If the collapse pressure is high enough, the corresponding low surface tension in the monolayer makes the monolayer unstable to undulations arising from events such as external vibrations or convection in the subphase, resulting in a bulk fracture and buckling of the monolayer. This seems to be the case for phospholipids such as DPPC, which can attain very high surface pressures upon compression (data not shown). For dissociable surfactants, the electrostatic repulsion due to a highly ionized monolayer prior to collapse may result in an increase in the activation energy for collapse as well as an increased free energy of the resulting collapsed phase, both of which would inhibit their formation (Pezron et al., 1990). Based on the results of the Gouy-Chapman analysis, the ionization of the monolayer seems to be responsible for the shift to a fracturing mechanism in pure PA films on a buffered saline subphase. This has also been shown to occur for other fatty acids such as stearic and arachidic acid (Xu et al., 1982; Pezron et al., 1990); increasing the pH of the subphase to ionize fatty acid monolayers increases the collapse pressure and changes the shape of the collapsed phase from round at low pH to highly elongated and fracture-like at high pH (Siegel et al., 1992). Simply switching between a pure water and a buffered saline subphase serves to significantly increase the collapse pressure of pure PA monolayers as well.

The important point to note for both of these mechanisms (heterogeneous nucleation or bulk fracture) is the fact that for pure films the monolayer consists of a continuous sheet of solid phase prior to collapse. Thus, the occurrence of collapse at any point in the monolayer can effectively result in collapse of the entire film (in analogy to a weak link in a chain). If collapse nucleates at energetically favorable heterogeneous sites at low pressures, these nuclei can act as sinks for the build-up of the collapsed phase for the entire monolayer, meaning that the homogeneous collapse pressure of the monolayer will never be reached. The partitioning of the condensed phase domains by the protein network reduces the likelihood of finding a heterogeneous nucleation site within a given condensed domain (Adamson, 1990). This phenomenon is the two-dimensional analog of the classic experiments of Turnbull, who showed that many simple metallic liquids could be undercooled far below their thermodynamic melting points (Turnbull, 1952). By subdividing the liquid into micron-size droplets, Turnbull was able to reduce the likelihood of heterogeneous nuclei in a given droplet, leading to homogeneous nucleation at large undercooling. Similar effects have been observed for supercooling water in emulsion droplets, polymer gels, or porous media (Tanaka et al., 1977; Bruggeller and Mayer, 1980). For PA monolayers in the presence of protein, the lc domains appears to be of uniform tilt when viewed with BAM, eliminating the effect of any residual defect points acting as heterogeneous nucleation sites upon transition to the solid phase. Also, each condensed domain must effectively initiate collapse independent of the others; if a heterogeneous site happens to exist in a given domain, then that domain may collapse at a low pressure, but collapse will not be able to propagate to the rest of the monolayer.

The network can also serve to inhibit the bulk fracturing process. For these films, long wavelength undulations in the interface that trigger collapse in pure solid films may not be able to act on the smaller domains in the protein-containing films. The length of propagation of any fractures in the film can also be limited by the protein network, effectively causing each domain to initiate collapse independently. Based on the length scales of the fracture cracks observed in the pure PA films, the fracturing process appears to be an event of high cooperativity, which may explain the reversion of the collapse mechanism to a nucleation process in the protein-containing films on a buffered saline subphase.

Re-expanding a collapsed film of pure PA inevitably leads to an offset in the subsequent isotherm obtained upon recompression, most likely due to the kinetically limited respreading of the macroscopic collapsed phase. For pure PA films on a pure water subphase, the collapsed domains are tilted (as evidenced via PFM and BAM), indicating that the collapsed domains have a more expanded structure than the underlying monolayer. It is thus not surprising that the collapsed domains do not readily reinsert upon expansion, since they would have to increase their packing density to do so. For protein-containing films, the growth of the collapse structures is limited by the finite size of the condensed domains, hence respreading these small collapse structures on expansion occurs much more readily. Also, if the protein is present in the collapsed phase to some extent, it may inhibit the ordered packing of the collapsed phase (which is also evidenced by the lack of observation of any tilt contrast

in the collapsed domains via BAM) and increase its free energy. As a result, the activation energy for collapse as well as the free energy of the collapsed phase itself are both increased. Thus, the barrier to collapse is increased, while the barrier to respreading is decreased, leading to a more collapse-resistant, yet respreadable, film. The collapsed phase in the presence of protein may be more similar in structure to the underlying monolayer, which may facilitate its reincorporation; the protein-rich network itself may also provide sites for easier reincorporation. It is therefore clear that one function of SP-B is to form a network of fluid phase that breaks up the condensed phase domains, thereby altering the nucleation and growth of monolayer collapse, leading to lower ultimate surface tensions on compression and easier respreading on expansion.

CONCLUSION

We have shown that the addition of SP-B protein to PA monolayers has a drastic effect on their properties and surface morphology. Fluorescence, polarized fluorescence, and Brewster angle microscopies revealed that both full-length SP-B and its amino terminus fluidize PA monolayers and increase their collapse pressure, effectively removing the driving force for the squeeze-out of the fatty acid from the lung surfactant monolayer. This is accomplished by the formation of a fluid network that segregates condensed phase domains at all surface pressures. The use of a dual-probe system showed that the newly created fluid phase was rich in protein, indicating the preference of the protein to partition into the less-ordered phase. The driving force for the formation of the network appears to be a low-line tension between the protein-rich and condensed phases, as evidenced by the results of a Gouy-Chapman analysis of the system and the observation of stripe phases under certain conditions. This network appears to perform three critical functions to convert the PA isotherm into one better suited for lung surfactant: 1) the monolayer is more compressible at all surface pressures; 2) collapse proceeds via a different mechanism in the presence of protein, switching from irreversible, heterogeneous nucleation and growth and bulk fracturing mechanisms to a more reversible, homogeneous mechanism; 3) this alteration in the collapse mechanism reduces the sizes of the collapse domains, making it easier to reincorporate the collapsed material into the monolayer on respreading. The synergistic interactions of SP-B and other lung surfactant proteins with anionic components of lung surfactant results in the formation of a monolayer with properties well suited for LS.

REFERENCES

Adamson, A. W. 1990. Physical Chemistry of Surfaces. 5th ed. John Wiley & Sons, New York.

Benvegnu, D. J., and H. M. McConnell. 1992. Line tension between liquid domains in lipid monolayers. *J. Phys. Chem.* 96:6820–6824.

Bibo, A., and I. Peterson. 1990. Phase diagrams of monolayers of the long chain fatty acids. *Adv. Mat.* 2:309–311.

Bruggeller, P., and E. Mayer. 1980. Complete vitrification in pure liquid water and dilute aqueous solutions. *Nature* 288:569–570.

Cochrane, C., and S. Revak. 1991. SP-B: structure-function relationships. *Science* 254:566–568.

Cockshutt, A., D. Absolom, and F. Possmayer. 1991. The role of palmitic acid in pulmonary surfactant: enhancement of surface activity and prevention of inhibition by blood proteins. *Biochim. Biophys. Acta.* 1085: 248–256.

De Keyser, P., and P. Joos. 1984. Kinetics of monolayer collapse as a nucleation process. *J. Phys. Chem.* 88:274–280.

Fields, C., D. Lloyd, R. Macdonald, K. Ottenson, and R. Noble. 1991. HBtu activation for automated Fmoc solid-phase synthesis. *Pept. Res.* 4:95–101.

Fleming, B., and K. M. W. Keough. 1988. Surface respreading after collapse of monolayers containing major lipids of pulmonary surfactant. *Chem. Phys. Lipids.* 49:81–86.

Fujiwara, T. 1992. Pharmacology of exogenous surfactant. *In* Pulmonary Surfactant: From Molecular Biology to Clinical Practice. L. M. J. Van Golde and J. J. Batenburg, editors. Elsevier, Amsterdam. 561–592.

Gordon, L. M., S. Horvath, M. L. Longo, J. A. Zasadzinski, H. W. Taeusch, K. Faull, C. Leung, and A. J. Waring. 1996. Conformation and molecular topography of the N-terminal segment of surfactant protein B in structure-promoting environments. *Protein Sci.* 5:1662–1675.

Gorree, G., J. Egberts, G. Bakker, A. Beintema, and M. Top. 1991. Development of a human lung surfactant derived from extracted amniotic fluid. *Biochim. Biophys. Acta.* 1086:209–216.

Hawgood, S., and K. Shiffer. 1991. Structures and properties of the surfactant-associated proteins. *Annu. Rev. Physiol.* 53:375–394.

Helm, C., L. Laxhuber, M. Lösche, and H. Möhwald. 1986. Electrostatic interactions in pholpholipid membranes I: influence of monovalent ions. *Coll. Poly. Sci.* 264:46–55.

Hénon, S., and J. Meunier. 1991. Microscope at the Brewster angle: direct observation of first-order phase transitions in monolayers. *Rev. Sci. Instr.* 62:936–939.

Hönig, D., and D. Möbius. 1991. Direct visualization of monolayers at the air-water interface by BAM. *J. Phys. Chem.* 95:4590–4592.

Ikegami, M., Y. Agata, T. Elkady, M. Hallman, D. Berry, and A. Jobe. 1987. Comparison of four surfactants: in vitro surface properties and responses of preterm lambs to treatment at birth. *Pediatrics.* 79:38–46.

Knobler, C. M. 1990. Seeing phenomena in flatland: studies of monolayers by fluorescence microscopy. *Science.* 249:870–874.

Knobler, C. M., and R. Desai. 1992. Phase transitions in monolayers. *Annu. Rev. Phys. Chem.* 43:207.

Lipp, M. M., K. Y. C. Lee, J. A. Zasadzinski, and A. J. Waring. 1996. Phase and morphology changes induced by SP-B protein and its amino-terminal peptide in lipid monolayers. *Science.* 273:1196–1200.

Lipp, M. M., K. Y. C. Lee, J. A. Zasadzinski, and A. J. Waring. 1997. Design and performance of an integrated fluorescence, polarized fluorescence, and Brewster angle microscope/Langmuir trough assembly for the study of lung surfactant monolayers. *Rev. Sci. Instr.* In press.

Longo, M. L., A. Bisagno, J. A. Zasadzinski, R. Bruni, and A. J. Waring. 1993. A function of lung surfactant protein SP-B. *Science.* 261:453–456.

Lösche, M., and H. Möhwald. 1989. Electrostatic interactions in phospholipid membranes II: influence of divalent ions on monolayer structure. *J. Coll. Int. Sci.* 131:56–67.

McConnell, H. M. 1989. Theory of hexagonal and stripe phases in monolayers. *Proc. Natl. Acad. Sci. USA.* 86:3452–3455.

McConnell, H. M. 1991. Structures and transitions in lipid monolayers at the air-water interface. *Annu. Rev. Phys. Chem.* 42:171–195.

McConnell, H. M., and R. D. De Koker. 1996. Equilibrium thermodynamics of lipid monolayer domains. *Langmuir.* 12:4897–4904.

McLean, L., J. Krstenansky, R. Jackson, K. Hagaman, K. Olsen, and J. Lewis. 1992. Mixtures of synthetic peptides and dipalmitoylphosphatidylcholine as lung surfactants. *Am. Physiol. Soc.* 92:L292–L300.

Möhwald, H. 1993. Surfactant layers at water surfaces. *Rep. Prog. Phys.* 56:653–685.

Möhwald, H., A. Dietrich, C. Bohm, G. Brezesinski, and M. Thoma. 1995. Domain formation in monolayers. *Mol. Mem. Biol.* 12:29–38.

Moore, B., C. M. Knobler, S. Akamatsu, and F. Rondelez. 1990. Phase diagram of Langmuir monolayers of pentadecanioc acid: quantitative comparison of surface pressure and fluorescence microscopy results. *J. Phys. Chem.* 94:4588–4595.

Muller, P., and F. Gallet. 1992. Ordered domains in a Langmuir monolayer: structure and line energy. *Thin Solid Films.* 210/211: 138–140.

Nag, K., C. Borland, N. Rich, and K. M. W. Keough. 1991. Epifluorescence microscopic observation of monolayers of dipalmitoylphosphatidylcholine: dependence of domain size on compression rates. *Biochim. Biophys. Acta.* 1068:157–160.

Nag, K., and K. M. Keough. 1993. Epifluorescence microscopic studies of monolayers containing mixtures of dioleoyl- and dipalmitoylphosphatidylcholines. *Biophys. J.* 65:1019–1026.

Nag, K., N. Rich, and K. Keough. 1994. Interaction between dipalmitoylphosphatidylglycerol and phosphatidylcholine and calcium. *Thin Solid Films.* 244:841–844.

Pastrana-Rios, B., C. Flach, J. Brauner, A. Mautone, and R. Mendelsohn. 1994. A direct test of the "squeeze-out" hypothesis of lung surfactant function: external reflection FT-IR at the air/water interface. *Biochemistry.* 33:5121–5127.

Perez-Gil, J., K. Nag, S. Taneva, and K. M. W. Keough. 1992. Pulmonary surfactant protein SP-C causes packing rearrangements of dipalmitoylphosphatidylcholine in spread monolayers. *Biophys. J.* 63:197–204.

Peterson, I. 1992. Phases of amphiphilic monolayers in different environments. *Phys. Scr.* T45:245–247.

Pezron, E., P. M. Claesson, J. M. Berg, and D. Vollhardt. 1990. Stability of arachidic acid monolayers on aqueous salt solutions. *J. Coll. Int. Sci.* 138:245–254.

Possmayer, F. 1988. A proposed nomenclature for pulmonary surfactant-associated proteins. *Am. Rev. Respir. Dis.* 138:990–998.

Riviere, S., S. Hénon, and J. Meunier. 1995. Electrostatic pressure and line tension in a Langmuir monolayer. *Phys. Rev. Lett.* 75:2506–2509.

Schwartz, R., M. Anastasia, M. Luby, J. Scanlon, and R. Kellogg. 1994. Effect of surfactant on morbidity, mortality, and resource use in newborn infants weighing 500 to 1500 g. *N. Engl. J. Med.* 330:1476–1480.

Schwartz, D. K., and C. M. Knobler. 1993. Direct observations of transitions between condensed Langmuir monolayer phases by polarized fluorescence microscopy. *J. Phys. Chem.* 97:8849–8851.

Seul, M., and D. Andelman. 1995. Domain shapes and patterns: the phenomonology of modulated phases. *Science.* 267:476–483.

Shapiro, D. L. 1989. Development of surfactant replacement therapy. *In* Surfactant Replacement Therapy. D. L. Shapiro and R. H. Notter, editors. Liss, New York. 1–18.

Shiffer, K., S. Hawgood, H. Haagsman, B. Benson, J. Clements, and J. Goerke. 1993. Lung surfactant proteins, SP-B and SP-C, alter the thermodynamic properties of phospholipid membranes—a differential calorimetry study. *Biochemistry.* 32:590–597.

Siegel, S., D. Hönig, D. Volhardt, and D. Möbius. 1992. Direct observation of three-dimensional transformation of insoluble monolayers. *J. Phys. Chem.* 96:8157–8160.

Smith, R., and J. Berg. 1980. The collapse of surfactant monolayers at the air-water interface. *J. Coll. Int. Sci.* 74:273–286.

Tanaka, T., S. Ishiwata, and C. Ishimoto. 1977. Critical behavior of density fluctuations in gels. *Phys. Rev. Lett.* 38:771–774.

Tanaka, Y., and T. Tsunetomo. 1983. Lung surfactants I. Comparison of surfactants prepared from lungs of calf, ox, dog, and rabbit. *Chem. Pharm. Bull.* 31:4091–4099.

Tanaka, Y., T. Tsunetomo, and K. Masuda. 1983. Lung surfactants III. Correlations among activities in vitro, in situ, and in vivo, and chemical composition. *Chem. Pharm. Bull.* 31:4110–4115.

Tanaka, Y., T. Tsunetomo, A. Toshimitsu, K. Masuda, K. Akira, and T. Fujiwara. 1986. Development of synthetic lung surfactants. *J. Lipids Res.* 27:475–485.

Taneva, S., and K. Keough. 1994. Dynamic surface properties of pulmonary surfactant proteins SP-B and SP-C and their mixtures with dipalmitoylphosphatidylcholine. *Biochemistry.* 33:14660–14670.

Turnbull, D. 1952. Kinetics of solidification of supercooled liquid mercury droplets. *J. Chem. Phys.* 20:411.

Waring, A. J., H. W. Taeusch, R. Bruni, J. Amirkhanian, B. Fan, R. Stevens, and J. Young. 1989. Synthetic amphipathic sequences of surfactant protein-B mimic several physicochemical and in vivo properties of native pulmonary surfactant proteins. *Pept. Res.* 2:308–313.

Weaver, T., and J. Whitsett. 1991. Function and regulation of expression of pulmonary surfactant-associated proteins. *Biochem. J.* 273:249–264.

Xu, S., K. Miyano, and B. Abraham. 1982. The effect of pH on monolayer stability. *J. Coll. Int. Sci.* 89:581–583.